

First-Principles Property Assessment of Hybrid Formate Perovskites

Abduljelili Popoola¹, P. S. Ghosh^{2,3}, Maggie Kingsland¹, Ravi Kashikar¹, D. DeTellem¹, Yixuan Xu⁴, S. Ma⁴, S. Witanachchi¹, S. Lisenkov¹, and I. Ponomareva¹

1. Department of Physics, University of South Florida, Tampa, Florida 33620, USA

2. Glass & Advanced Materials Division, Bhabha Atomic Research Centre, Mumbai 400 085, India

3. Homi Bhabha National Institute, Anushaktinagar, Mumbai 400 094, India and

4. Department of Chemistry, University of North Texas,
CHEM 305D, 1508 W Mulberry Street, Denton, Texas 76201, USA

Hybrid organic inorganic formate perovskites, $\text{AB}(\text{HCOO})_3$, is a large family of compounds which exhibit variety of phase transitions and diverse properties. Some examples include (anti)ferroelectricity, ferroelasticity, (anti)ferromagnetism, and multiferroism. While many properties of these materials have already been characterized, we are not aware of any study that focuses on comprehensive property assessment of a large number of formate perovskites. Comparison of the materials property within the family is challenging due to systematic errors attributed to different techniques or the lack of data. For example, complete piezoelectric, dielectric and elastic tensors are not available. In this work, we utilize first-principles density functional theory based simulations to overcome these challenges and to report structural, mechanical, dielectric, piezoelectric, and ferroelectric properties for 29 formate perovskites. We find that these materials exhibit elastic stiffness in the range 0.5 to 127.0 GPa, highly anisotropic linear compressibility, including zero and even negative values; dielectric constants in the range 0.1 to 102.1; highly anisotropic piezoelectric response with the longitudinal values in the range 1.18 to 21.12 pC/N, and spontaneous polarizations in the range 0.2 to 7.8 $\mu\text{C}/\text{cm}^2$. Furthermore, we propose and computationally characterize a few formate perovskites, which have not been reported yet.

Hybrid organic inorganic perovskites (HOIP) are receiving a lot of attention presently owing to the rapid progress in their synthesis and characterization. They have the chemical formula ABX_3 , where A is typically an organic molecule, B is a metallic cation, while X site could be halogen or molecular linker. They exhibit a variety of phase transitions and rich range of properties, such as ferromagnetism, (diel/ferro)electricity, non-linear optical properties, caloric effects, ferroelasticity, multiferroicity, among others [1, 2]. Among chemically diverse HOIPs, $\text{AB}(\text{HCOO})_3$, is one of the largest families, where one can find most of the aforementioned properties. The structural phase transitions in these materials are primarily driven by the hydrogen bond stabilization and often occur close or even above room temperature, which is highly desirable feature [1]. For example, most ethyl ammonium metal formate perovskites exhibit transition in the range 293 to 400 K [3–6]. Magnetic properties of formates are mostly determined by weak magnetic interactions mediated by formate linker causing them to exhibit magnetic ordering at low temperatures only, typically below 50 K [1]. Furthermore, $[\text{AZE}][\text{M}(\text{HCOO})_3]$ (AZE = azetidinium; M = Mn^{2+} , Cu^{2+} and Zn^{2+}) family was reported to have extraordinarily large dielectric constants higher than 10^4 in the vicinity of room temperature [7–9]. Often times, the value exhibit strong frequency dependence, which resemble behavior of ferroelectric relaxors [10]. Many formates undergo transitions into polar space groups and, therefore, are possible candidates for ferroelectricity, which is defined by the presence of spontaneous electric polarization reversible by electric field. However, the value of spontaneous polarization is typically below 5 $\mu\text{C}/\text{cm}^2$, which makes its experimen-

tal measurement very challenging [11]. Table II provides polarization values from the literature and conditions for which it was reported/computed. The simultaneous realization of ferroelectricity, ferromagnetism and/or ferroelasticity in some hybrid formates classify them as multiferroics. It was shown that DMA-Zn(HCOO)₃ becomes multiferroic on substitution of Zn with transition metals such as Ni, Mn, Co and Fe [2, 12, 13]. DMA-Co(HCOO)₃ is another hybrid in which multiferroicity has been observed [14]. All abbreviations for A sites used in this study are listed in Table I.

Mechanical properties have been investigated for several members of formate families and are reviewed in Ref.[35]. Some representative data from the literature for Young's and elastic moduli are compiled in Table III. The exotic negative linear compressibility, defined as an increase in lattice parameter(s) under hydrostatic pressure, has been computationally predicted in HAZ-M(HCOO)₃ (M = Mn,Fe,Co) [36, 37] and NH₄Zn(HCOO)₃ [38]. Negative linear compressibility finds applications in pressure sensors and actuators, and possibly in design of artificial muscles[39].

Evidences of pyroelectricity have reported in some hybrid formates perovskites. For instance, pyroelectric coefficient was measured to exhibit a maximum of 5.16×10^{-2} C/m² K under a poling electric field of 7.7 kV/cm at 192 K for DMA-Mn(HCOO)₃ [19]. In another instance, pyroelectric current was reported and used to study the order-disorder transition under different pressures in DMA-Co(HCOO)₃ [21]. Some other hybrid formates perovskites in which pyroelectric current has been measured include DMA-Mg(HCOO)₃ [43], DMA-Mn(HCOO)₃, DMA-Mn_{0.5}Ni_{0.5}(HCOO)₃ [17, 18],

TABLE I. Abbreviations for A sites used in the study, following Stroppas book[1]

Material abbreviation	NH ₂ NH ₃ HAZ	C ₂ H ₅ NH ₃ EA	C(NH ₂) ₃ Gua	(CH ₃) ₂ NH ₂ DMA	CH ₃ NH ₃ MA	NH ₂ CHNH ₂ FA
-----------------------	--	---	---	--	---------------------------------------	---

TABLE II. Polarizations from literature and those computed in this work. A = NH₃CH₂CH₃, P = PH₃CH₂CH₃, AF = NH₃CH₂CF₃, PF = PH₃CH₂CF₃.

Material	Type	Literature	Conditions	P ($\mu\text{C}/\text{cm}^2$)
A-Mn	Comp.	1.80 ^[15]	T = 0 K	–
P-Mn	Comp.	1.00 ^[15]	T = 0 K	–
AF-Mn	Comp.	5.10 ^[15]	T = 0 K	–
PF-Mn	Comp.	5.90 ^[15]	T = 0 K	–
DMA-Mn	Exp.	0.30 ^[16]	T = 150 K; B = 9 T (during growth)	7.52
	Exp.	2.70 – 3.61 ^[17, 18]	T = 150 K; B = 0 – 5 T; E = 5 kV/cm	–
	Exp.	0.8-2.4 ^[19]	T = 184 K; E = 3.1-7.7 kV/cm	–
DMA-Ni	Exp	0.42 – 0.52 ^[20]	T = 150 K; B = 0 – 10 T	–
DMA-Co	Exp.	0.30 ^[21]	T = 125 K	7.44
DMA-Zn	Exp.	0.45 ^[22]	T = 125 K	7.77
NH ₄ Mn	Exp.	0.97 ^[23]	T = 140 K	2.45
NH ₄ Mg	Exp.	1.15 ^[3]	T = 93 K	–
NH ₄ Zn	Exp.	0.02 – 0.93 ^[24]	T = 120 – 248 K	2.43
	Exp.	4.00 ^[25]	T = 273 K; P = 1.44 GPa	–
	Exp.	1.03 ^[23, 26]	T = 163 K	–
NH ₄ Sc	Comp.	3.71 ^[27]	T = 0 K	–
NH ₄ Ti	Comp.	2.46 ^[27]	T = 0 K	–
NH ₄ V	Comp.	2.40 ^[27]	T = 0 K	–
NH ₄ Cr	Comp.	2.51 ^[27]	T = 0 K	–
NH ₄ Mn	Comp.	2.38 ^[27]	T = 0 K	–
NH ₄ Fe	Comp.	2.37 ^[27]	T = 0 K	–
NH ₄ Co	Comp.	2.36 ^[27]	T = 0 K	–
NH ₄ Ni	Comp.	2.17 ^[27]	T = 0 K	2.27
NH ₄ Cu	Comp.	2.20 ^[27]	T = 0 K	–
NH ₄ Zn	Comp.	2.30 ^[27]	T = 0 K	2.43
CH ₃ NH ₂ NH ₂ Mn	Exp.	0.14 ^[28]	T = 150 K; B = 10 T	–
NH ₃ (CH ₂) ₄ NH ₃ Mg ₂	Exp.	1.51 ^[3]	T = 93 K	–
HAZ-Mn	Exp. (estimated)	3.58 ^[29]	T = 110 K	2.17
HAZ-Co	Exp. (estimated)	2.61 ^[29]	T = 405 K	2.53
HAZ-Zn	Exp. (estimated)	3.48 ^[29]	T = 110 K	2.32
HAZ-Mg	Exp. (estimated)	3.44 ^[29]	T = 400 K	2.53
	Comp.	2.6 ^[30]	T = 150 – 375 K	2.53
EA-Mg	Exp. (estimated)	3.43 ^[3]	T = 93 K	1.26
Gua-Cr	Comp.	0.22 ^[31]	T = 0 K	–
Gua-Cu _{0.5} Mn _{0.5}	Comp.	9.90 ^[32]	T = 0 K	–
Gua-Cu	Comp.	0.11 - 0.37 ^[33, 34]	T = 0 K	0.21

Gua-Cu(HCOO)₃ [33], CH₃NH₂NH₂Mn(HCOO)₃ [28] and DMA-Zn(HCOO)₃ [22]. The dependence of pyroelectric current on applied magnetic field has also been demonstrated in DMA-Ni(HCOO)₃ [20].

Although, the aforementioned studies highlight the outstanding progress that has been made in characterization of these materials, the survey also reveals scarcity of such investigations, especially in the light of the fact that formates subgroup hosts at least 64 known members [1, 44, 45]. It should also be recognized that many

such characterizations, spontaneous polarization for example, are rather challenging experimentally. On the other hand, computational investigation is an inexpensive, reliable and efficient tool to overcome these challenges and achieve a comprehensive assessment of structural, piezoelectric, dielectric and elastic properties for a wide range of materials in the formate family.

Therefore, in this study, we aim: (i) to predict structural parameters, polarization, piezoelectric coefficients, dielectric constants and elastic stiffness of 29 formate

TABLE III. Elastic properties from the literature. AZE = $(\text{CH}_2)_3\text{NH}_2$

Material	Type	Young's Moduli (GPa)	Elastic Moduli (GPa)	Ref.
DMA-Ni	Exp.	24.5		[35]
DMA-Mn	Exp.	19.0		[35]
DMA-Co	Exp.	21.5		[35]
DMA-Zn	Exp.	19.0		[35]
Gua-Cu	Exp.		15.0 – 21.0	[40]
Gua-Zn	Exp.		24.0 – 29.0	[40]
Gua-Mn	Exp. & Comp.		23.5(6) – 28.6(4)	[41]
AZE-Cu	Exp. & Comp.		11.5(4) – 12.6(3)	[41]
HAZ-Zn	Exp.		24.5 – 26.5	[42]
HAZ-Mn	Exp.		24.5 – 28.6	[42]
NH ₄ Zn	Exp. & Comp.		18.2 – 34.4	[38]

compounds using first-principles density functional theory (DFT) based simulations; (ii) to provide a comprehensive comparative assessment of the aforementioned properties; (iii) to catalog the properties which could aid screening of promising materials.

I. COMPUTATIONAL METHODOLOGY

Table IV lists the hybrid formates that we have investigated and the associated experimental references from which the structures have been retrieved along with temperatures at which the structures were recorded. The bottom part of the panel lists some of the HOIPs in the same family, which did not become part of this study. The experimental structures were used to initialize DFT based computations as implemented in VASP package [58–61]. Technically, all experimental structures were first fully relaxed using Perdew-Burke-Ernzerhof (PBE) version of the generalized gradient approximation for exchange correlation functional [62]. In order to model hydrogen bonds, we used dispersion corrections of zero-damping D3 [63, 64], which was previously shown to provide good agreement with experimental structures [65–69]. The electron-ion interactions are treated with the projected augmented wave (PAW) potentials [70]. We used the plane wave cutoff energy in range 700–850 eV and non-Gamma centered k-point mesh which corresponds to k-point densities in range 0.19 – 0.57 Å⁻¹. Note that k-point density and cutoff energy for each material are given in Table S1 in supplementary material. The Hubbard correction as proposed by Dudarev *et al.* [71] is introduced to account for the Coulomb repulsion between localized d-electrons of transition metals. Unit cell parameters and atomic positions were relaxed until stress and forces are less than 0.1 GPa and 1 meV/Å, respectively. The energy convergence criterion for self-consistent calculations was 10⁻⁶ eV. The crystal polarization is evaluated by the Berry phase method developed by King-Smith and Vanderbilt [72, 73]. We computed the *intrinsic* piezoelectric constants e_{ij} and d_{ij} (in matrix notations) defined as the linear response of the po-

larization to the applied strain and stress, respectively. The d_{ij} coefficients were obtained from $d_{ij} = e_{ik}(C^{-1})_{kj}$, where C is the single crystal elastic constant matrix. The constants e_{ik} and C_{ij} were computed using finite difference method as implemented in VASP [74]. Hubbard U were employed for transition metal atoms. The following values computed using the linear response ansatz of Cococcioni *et al* [75] from PAW approach in VASP were utilized: 6.5 eV for Mn, 7.2 eV for Fe , 4.6 eV for Co and 5.1 eV for Ni.

II. RESULTS AND DISCUSSION

A. Structure

The ground state structural parameters are reported in Table V. Comparison with experimental data, where available, was also provided in the table. We find that, in most cases, the lattice parameters are within 1% of experimental (see Supplementary material, Table S1). The pictorial representation of how experimental lattice parameters compare with computational ones is given in Fig. 1. The figure reveals good agreement between experiment and computations. We thus conclude that our computational approach provide reliable structural predictions. The ground state structures are available from Ref.[76].

Note, that we also augmented our list of HOIPs with the following structures DMA-Zn, DMA-Co, HONH₃-Fe and Pna₂1 phase of HAZ-Mg, which so far have not been reported experimentally. Such structures were obtained by replacing Mn in DMA-Mn with Zn or Co, Mn in HONH₃-Mn with Fe, and Zn in HAZ-Zn with Mg, followed by full structural relaxation. These hypothetical structures are underscored in Table IV. Majority of the fully relaxed HOIPs structures retained their experimental space groups. However, there were some exceptions. The experimental structures of MA-Co are available in both Pnma and P2₁/c phases whereas experimental structures of MA-(Mn,Zn) are available only in Pnma phase. Our computations predicted that MA-

TABLE IV. Materials investigated in this study (upper part of the Table). The underscored compounds do not have experimental structure available from the literature. The bottom part of the Table gives other materials from the same family, which are not part of this investigation.

Material	Space Group	T (K)	Experimental Ref.
Gua-M ($M = \text{Co, Fe, Mn, Ni, Zn}$)	Pnma	293	[46]
Gua-Cu	Pna ₂ ₁	293	[46]
EA-Mg	Pna ₂ ₁	292	[3]
DMA-M ($M = \text{Co, Mn, Zn}$)	Cc	285	[47]
MA-M ($M = \text{Mn, Zn, Co, Ni}$)	Pnma	135, 290, 290, 100	[48–50]
HONH ₃ M ($M = \text{Co, Mg, Mn, Ni, Zn, Fe}$)	P2 ₁ 2 ₁ 2 ₁	293	[51]
FA-Mn	C2/c	110	[52]
HAZ-M ($M = \text{Mn, Zn, Co}$)	Pna ₂ ₁	110, 110, 298	[29, 53]
HAZ-M ($M = \text{Mg}$)	P2 ₁ 2 ₁ 2 ₁	110	[29]
NH ₄ M ($M = \text{Co, Fe, Mn, Zn}$)	P6 ₃	110	[23]
Gua-M ($M = \text{Cd}$)	R̄3c	150	[54]
Gua-M ($M = \text{Zn}$)	Pnma	120	[55]
NH ₄ M ($M = \text{Cu}$)	P2 ₁ 2 ₁ 2 ₁	120	[56]
NH ₄ M ($M = \text{Mg}$)	P6 ₃	93	[57]

TABLE V. Structural properties and polarizations. Ground state magnetic ordering of magnetic materials is in parenthesis, where FM and AFM denote ferromagnetic and antiferromagnetic orderings, respectively. The data in parenthesis give experimental values taking from the reference given in the last column.

material	space group	a(Å)	b(Å)	c(Å)	β (°)	V (Å ³)	μ_B	\mathbf{P} ($\mu\text{C}/\text{cm}^2$)	ref
Gua-Mn (AFM)	Pnma	8.42 (8.52)	11.91 (11.98)	9.12 (9.06)	90	915 (925)	4.7	non-polar	[46]
Gua-Fe (AFM)	Pnma	8.35 (8.42)	11.78 (11.85)	8.98 (8.95)	90	883 (892)	3.8	non-polar	[46]
Gua-Co (AFM)	Pnma	8.28 (8.33)	11.64 (11.75)	8.99 (8.91)	90	866 (873)	2.8	non-polar	[46]
Gua-Ni (AFM)	Pnma	8.24 (8.26)	11.63 (11.64)	8.91 (8.83)	90	853 (850)	1.8	non-polar	[46]
Gua-Cu (AFM)	Pna ₂ ₁	8.50 (8.52)	9.07 (9.03)	11.27 (11.35)	90	869 (874)	0.6	(0, 0, 0.21) (0.11–0.37)	[33, 34, 46]
Gua-Zn	Pnma	8.27 (8.35)	11.66 (11.73)	8.99 (8.91)	90	868 (872)	0.0	non-polar	[46]
HONH ₃ -Mn (AFM)	P2 ₁ 2 ₁ 2 ₁	7.80 (7.81)	8.04 (7.96)	13.06 (13.17)	90	819 (819)	4.5	non-polar	[51]
HONH ₃ -Co (AFM)	P2 ₁ 2 ₁ 2 ₁	7.67 (7.68)	7.82 (7.76)	13.00 (13.02)	90	780 (776)	2.7	non-polar	[51]
HONH ₃ -Ni (AFM)	P2 ₁ 2 ₁ 2 ₁	7.59 (7.62)	7.98 (7.78)	12.80 (12.73)	90	775 (755)	1.8	non-polar	[51]
HONH ₃ -Fe (AFM)	P2 ₁ 2 ₁ 2 ₁	7.70	8.00	13.05	90	802	3.6	non-polar	
HONH ₃ -Zn	P2 ₁ 2 ₁ 2 ₁	7.65 (7.69)	7.83 (7.74)	13.18 (13.02)	90	790 (775)	0.0	non-polar	[51]
HONH ₃ -Mg	P2 ₁ 2 ₁ 2 ₁	7.67 (7.69)	7.89 (7.79)	12.73 (12.86)	90	770 (770)	0.0	non-polar	[51]
HAZ-Co (AFM)	Pna ₂ ₁	8.63 (8.65)	7.74 (7.76)	11.46 (11.55)	90	765 (776)	2.7	(0, 0, 2.81) (2.61 at 405 K)	[53]
HAZ-Mn (FM)	Pna ₂ ₁	8.99 (8.93)	7.83 (7.82)	11.66 (11.69)	90	820 (817)	4.7	(0, 0, 2.51) (3.58 at 110 K)	[29]
HAZ-Zn	Pna ₂ ₁	8.65 (8.66)	7.75 (7.72)	11.49 (11.48)	90	771 (768)	0.0	(0, 0, 2.59) (2.6–3.48 at 0–110 K)	[29, 30]
HAZ-Mg	Pna ₂ ₁	8.87	7.63	11.45	90	775	0.0	(0, 0, 2.90) (3.44 at 400 K)	[29]
HAZ-Mg	P2 ₁ 2 ₁ 2 ₁	8.00 (7.89)	13.90 (13.75)	7.28 (7.38)	90	809 (802)	0.0	non-polar	[29]
NH ₄ -Co (AFM)	P ₃	12.54 (12.59)	12.54 (12.59)	8.34 (8.22)	90	1136 (1128)	2.6	(0, 0, 2.35)	[23]
NH ₄ -Fe (AFM)	P6 ₃	12.58 (12.62)	12.58 (12.62)	8.57 (8.36)	90	1174 (1153)	3.8	(0, 0, 2.41)	[23]
NH ₄ -Mn (AFM)	P6 ₃	12.55 (12.67)	12.55 (12.67)	8.71 (8.54)	90	1189 (1187)	4.5	(0, 0, 2.45)	[23]
NH ₄ -Zn	P6 ₃	12.56 (12.59)	12.56 (12.59)	8.38 (8.20)	90	1144 (1126)	0.0	(0, 0, 2.43) (0.93–1.03 at 120–163 K)	[23, 24, 26]
MA-Co (AFM)	Pnma	8.18 (8.28)	11.67 (11.67)	8.28 (8.15)	90	790 (789)	2.8	non-polar	[49]
MA-Co (AFM)	P2 ₁ /c	8.25 (8.18)	11.69 (11.67)	8.20 (8.15)	93.6 (91.9)	789 (789)	2.8	non-polar	[49]
MA-Mn (AFM)	Pnma	8.39 (8.68)	11.93 (11.95)	8.42 (8.17)	90	843 (847)	4.7	non-polar	[48]
MA-Mn (AFM)	P2 ₁ /c	8.41	8.47	14.12	121.9	853	4.7	non-polar	
MA-Ni (AFM)	Pnma	8.15 (8.18)	11.62 (11.52)	8.24 (8.08)	90	781 (762)	1.8	non-polar	[50]
MA-Zn	Pnma	8.31 (8.41)	11.69 (11.71)	8.17 (8.10)	90	794 (798)	0.0	non-polar	[48]
MA-Zn	P2 ₁ /c	8.27	13.89	8.26	122.4	802	0.0	non-polar	
DMA-Co (AFM)	Cc	14.10	8.24	8.62	121	859	2.7	(6.93, 0, 2.70) (0.3 at 125 K)	[21]
DMA-Mn (AFM)	Cc	14.35 (14.35)	8.39 (8.32)	8.86 (8.88)	120.3	922 (912)	4.7	(7.10, 0, 2.48) (0.3–2.7 at 150–184 K)	[16–19, 47]
DMA-Zn	Cc	14.13	8.24	8.64	120.71	865	0.0	(7.30, 0, 2.66) (0.45 at 125 K)	[22]
EA-Mg	Pna ₂ ₁	8.82 (8.90)	8.12 (8.12)	11.73 (11.81)	90	840 (853)	0.0	(0, 0, 1.45) (3.34 at 93 K)	[3]
FA-Mn (AFM)	C2/c	13.12 (13.44)	8.86 (8.68)	8.23 (8.41)	118.1	859 (865)	4.7	non-polar	[52]

(Mn,Zn,Co) are mechanically unstable in Pnma phase while P2₁/c phase of MA-Co is mechanically stable. To ensure mechanical stability of MA-(Mn,Zn) we deformed the Pnma structure along the eigenvector associated with negative value of C_{44} and subjected such deformed structure to full structural relaxation, which resulted in P2₁/c structure. It is therefore plausible, that these materials may undergo another structural phase transition to

P2₁/c phase at low temperatures. Both P2₁/c and Pnma phases of MA-(Mn,Zn,Co) are reported in Table V and Ref. [76]. However, dielectric and mechanical properties were calculated from P2₁/c phase of the structures.

It has been reported in previous experimental studies that at low temperature, DMA-Zn crystallizes in space group Cc with no partial occupancy at N position and possesses crystal structure similar to DMA-Mn [77].

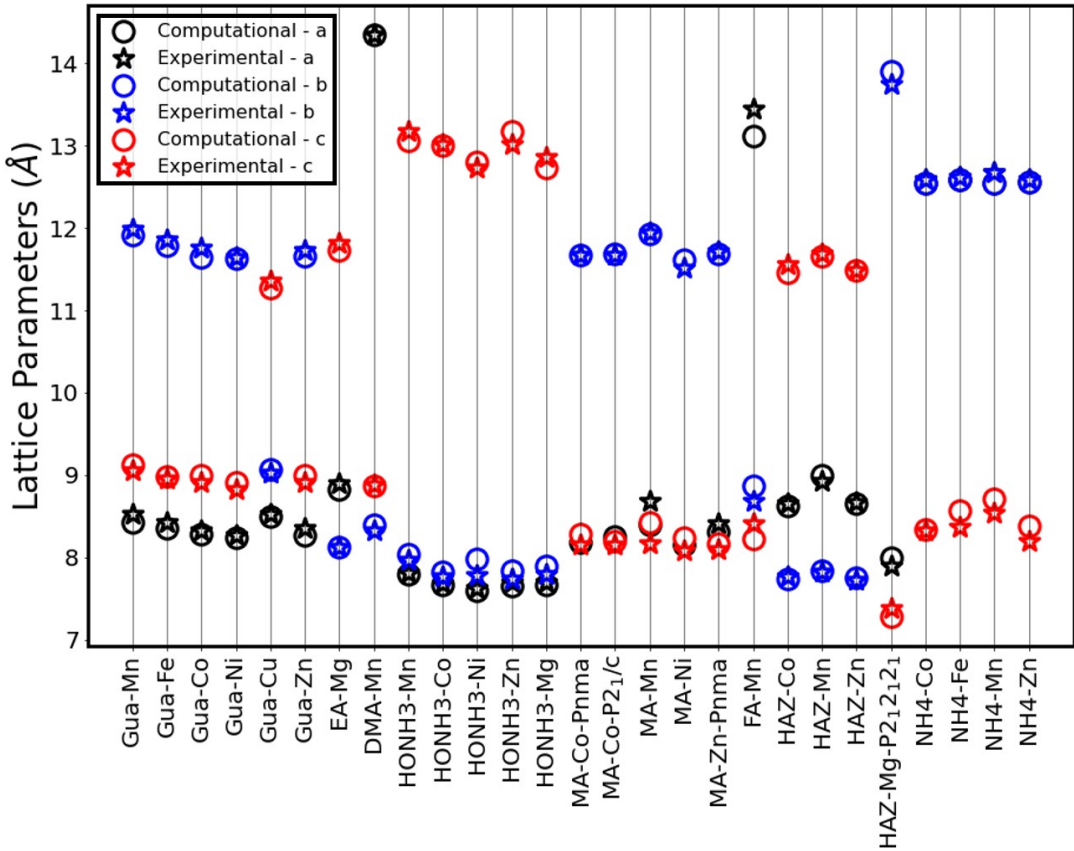


FIG. 1. Comparison between computational and experimental lattice parameters. Only the structures where space group is the same for both computations and experiment are compared.

However, no structural file has been provided. Therefore, we have initiated our calculation for DMA-Zn by replacing Mn with Zn in experimentally reported DMA-Mn [47]. In case of HAZ-Mg, previous experimental study reports a non-polar crystal structure P2₁2₁2₁ [29], but a recent DFT study [78] shows entropy driven effects are responsible for stabilizing the structure in Pna₂₁ space group. Therefore, we have initiated our calculation for Pna₂₁ phase of HAZ-Mg by replacing Zn with Mg in experimentally reported Pna₂₁ phase of HAZ-Zn [29].

NH₄-Co experimentally is reported in P6₃ space group at low temperature. However, relaxed structure in the same space group was found to be mechanically unstable so further relaxation resulted in P3 space group.

For all structures with transition metal atoms we computed energies for different magnetic orderings and selected the one with the lowest energy as the ground state. It should be noted that in agreement with previous studies[36, 37, 79], we find only very small differences in energy between structures with different magnetic orderings. The magnetic orderings are given in Table V.

B. Polarization

An inherent periodicity of crystal lattice makes polarization, \mathbf{P} , a multivalued quantity. To overcome this challenge the polarization is typically computed along a distortion path that connects polar structure to nonpolar one[80]. However, for the case of HOIP the nonpolar high symmetry structure is typically associated with partial occupancy and therefore cannot be used as a reference point. One approach to construct nonpolar phase was suggested in Ref.[81]. Another approach is to model experiments, where polarization is obtained from the measurement during its reversal. Such an approach was used in Ref.[68, 79], where the polarization reversal was achieved from creation of inverted structure and generating a roto-distortion path between the structure and its inversion. The inversion was applied with respect to the inversion center of high symmetry experimental structure, where available, or with respect to B-site. The roto-distortion path consists of distortion of the framework and rotation of the A site molecule. We used same approach for EA-M, HAZ-M, DMA-M as these compounds have inversion center in their high temperature phase. Example of polarization evolution along such a path is given in Fig. 2 (b) and Fig. 2 (c).

For Gua-Cu, rotations of the Gua molecules resulted in metallic structures, which did not allow for polarization calculations. So we created a non-polar structure using pseudosymmetry module of Bilbao Crystallographic server[82] and generated a distortion path between the polar and nonpolar structures. The polarization along such a path is given in Fig. 2(e). For NH₄-M family, the high temperature high symmetry structure is P6₃22 and does not have an inversion center. In this case, we used U2 axis of P6₃22 to generate the structure with reversed polarization direction. Technically, we applied the following transformation $x \rightarrow y$, $y \rightarrow x$ and $z \rightarrow -z$ on the Wykoff positions of NH₄-M in P6₃ phase. Note that for NH₄-Co, we report polarization for P6₃ phase, although it was found to be mechanically unstable in calculations. An example of polarization along such path is given in Fig. 2 (f).

Polarizations along the roto-distortion paths for all polar materials studied are given in Fig. S1 of Supplementary material, while the associated structures are given in Ref.[76]. The Figures also report the energy along the path. The energies are not likely to be physical as no optimization has been performed. However, they do reveal two minima, that is double-well potential. The typical barrier height is below 200 meV/atom which is considered surmountable[83]. The comparison of our results with experimental and computationally predicted values available from the literature can be found in Table II and Fig. 3. We find excellent agreement between our computational data and computational data from the literature. However, there exist discrepancies with experimental data. This could be attributed to the difference in temperature, and in some cases in phase, the difference in the direction of measurement. In our case we report the value along the polar direction. The data reveal that the polarization values for the formate family is in the range of 0.2-7.8 $\mu\text{C}/\text{cm}^2$ with largest values found in DMA-M. The values are a factor of ten lower than the ones for prototypical oxide ferroelectrics including BaTiO₃ and PbTiO₃ [84].

C. Piezoelectric response

The independent components of piezoelectric tensors, e_{ij} and d_{ij} , which are allowed by symmetry are given in Table VI and Table VII, respectively. Figure 4 provides comparative picture. For the formates with Pna₂₁ space group, we mostly find largest values for e_{15} and d_{15} components of the tensor. For materials in Cc and P2₁2₁2₁ space groups, the largest components are e_{35} (d_{35}) and e_{36} (d_{36}) respectively, and can reach 0.26 C/m^2 (25.36 pC/N) and 0.18 C/m^2 (14.64 pC/N) in DMA-Zn and HAZ-Mg, respectively. The longitudinal coefficients along the crystallographic directions, e_{ii} and d_{ii} , $i = 1, 2, 3$, range from 0.01 to 0.14 C/m^2 and 0.01 to 11.46 pC/N, respectively, with the largest of these values belonging to DMA-Zn. The transverse coefficients e_{ij} and d_{ij} , $i, j = 1,$

2, 3 are in the range 0.00 to 0.20 C/m^2 and 0.07 to 9.15 pC/N, respectively, with the largest values belonging to DMA-Zn.

The directional dependence of the longitudinal piezoelectric stress and strain responses was analyzed using MTex[85] and is presented in Fig. 5 and Fig. 6, respectively, for a representative material in each family. For all materials we find response to be highly anisotropic. The longitudinal piezoelectric stress coefficient can reach 0.22 C/m^2 in DMA-Co in $\langle \frac{1}{2}, 0, \frac{\sqrt{3}}{2} \rangle$ direction, while the strain coefficient can reach 12.93 pC/N in the vicinity of $\langle 1/2, 0, 1 \rangle$ direction. 3D visualizations of the piezoelectric stress/strain surfaces for the rest of the materials are given in Fig. S2 and Fig. S3 in the Supplementary material.

Thus, our data indicate that the intrinsic piezoelectric strain response in the formate family can reach 26.7 pC/N (in HAZ-Mn) for the shear stress component and 21.12 pC/N (in DMA-Zn along $\langle \frac{1}{2}, 0, \frac{\sqrt{3}}{2} \rangle$ direction) for the longitudinal one. DMA family exhibits the best values.

D. Dielectric response

The symmetry allowed components of the dielectric tensor are reported in Table IX. The typical value is 5. However, computations predict Gua-M to exhibit distinctively high values, up to 100.00, comparable in order of magnitude to dielectric constants of BaTiO₃[86]. The comparative view of the dielectric constants is given in Fig. 7, which confirm that Gua-M family exhibits largest response. The nature of such unusual response deserves further investigation.

E. Mechanical Properties

Mechanical properties describe the materials response to external mechanical stimuli, such as pressure, stress or strain. The independent components of stiffness tensors are given in Table VIII. They satisfy the Bohn conditions for the elastic stability [87, 88] as checked by VASPKIT[89]. The typical diagonal elements are in the range 3.3 to 127.0. Comparative view of the stiffness tensor components among all the formates is given in Fig. 8. We computed average Bulk modulus (B), Young modulus (E), shear modulus (G), Poisson's ratio (ν) and Cauchy's pressure (CP) for bulk polycrystals within the Hills' approximation as implemented in VASPKIT[89-95] and reported them in Table X. The values compare well with the experimental results, listed in Table III.

Poisson's ratio, defined as the ratio of transverse compressive strain to longitudinal tensile strain, and Pugh's ratio, commonly expressed as B/G ratio, can be used to characterize ductility or brittleness of crystals. The former one typically ranges from 0.0 to 0.5. Ductility-brittleness border line is usually drawn at Poisson ratio

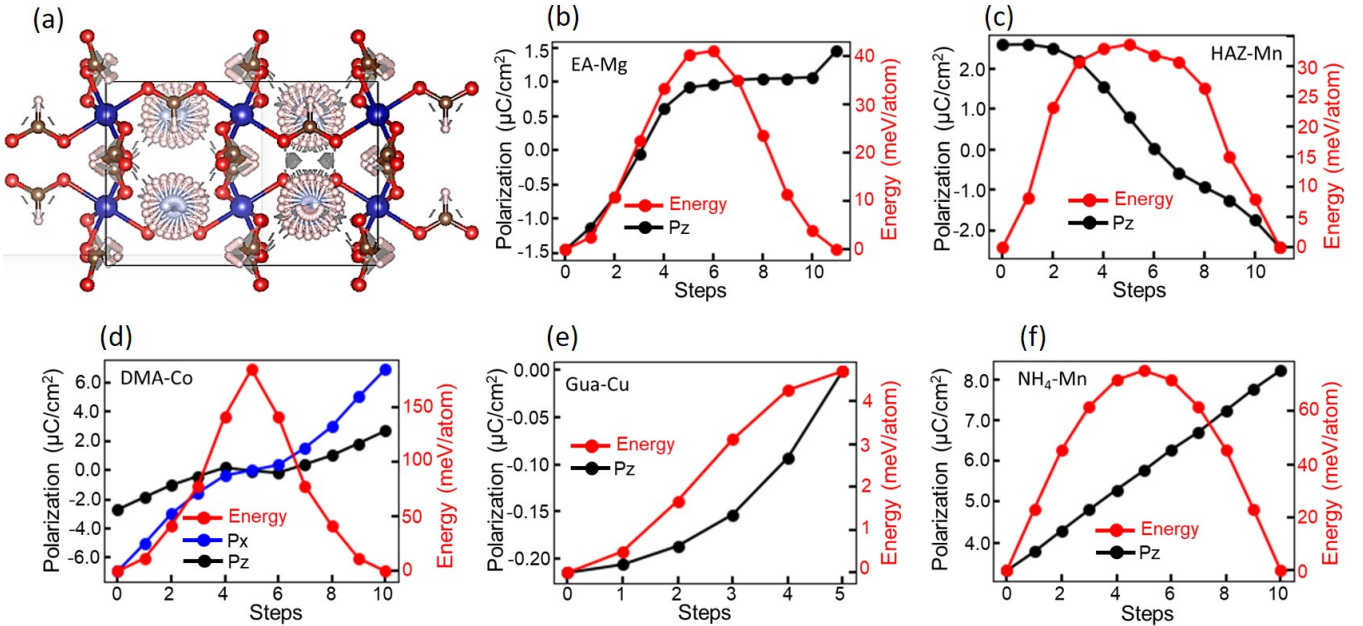


FIG. 2. Structural evolution along roto-distortion path schematically shown by overlapping structures along the path (a). Variation of polarization and energy along the path for a representative of each family, as given in the legend (b)-(f)

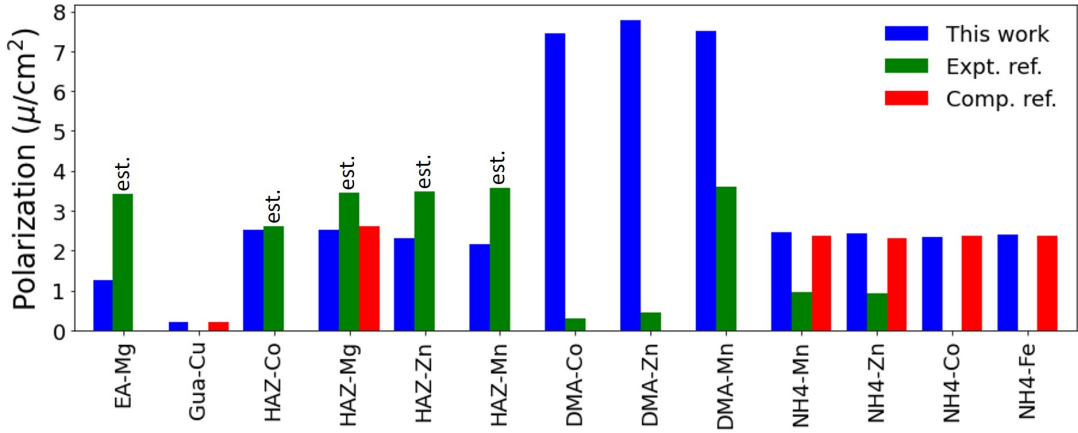


FIG. 3. Comparison of our computational polarization values with experimental and computational results from the literature[3, 16, 21–25, 29]. Note, "est." indicates that the polarization was estimated from the separation between positive and negative charge.

of 0.26 and at Pugh ratio of 1.75 [96, 97]. As shown in Fig. 9, most of the formates studied in this work are ductile and therefore are able to withstand large stresses and exhibit malleability.

Figure 10 shows the directional dependence of linear compressibility, defined as linear expansion or compression of materials upon application of isotropic pressure. Interestingly, the data predict that a few formates have negative values (indicated by red color) and some exhibit nearly zero values. For example, $\text{HONH}_3\text{-Ni}$, MA-Co and $\text{NH}_4\text{-Mn}$ exhibit negative values along $\langle 0, 1, 0 \rangle$, $\langle -0.6447, 0, -0.7644 \rangle$ and $\langle 0, 0, 1 \rangle$ directions, respectively. Directional dependence of linear compress-

ability for other materials are presented in supplementary material Fig. S4. Previously negative linear compressibility was predicted for HAZ-Co, HAZ-Mn, HAZ-Fe and $\text{NH}_4\text{-Zn}$ [36–38] and explained on the basis of strut-hinge model[98, 99].

III. CONCLUSION AND OUTLOOK

In summary, we have used DFT computations to assess structural, electric, piezoelectric, and mechanical properties of 29 hybrid formate perovskites. We predict that the ground state phase of most MA-M (M = Co, Mn,

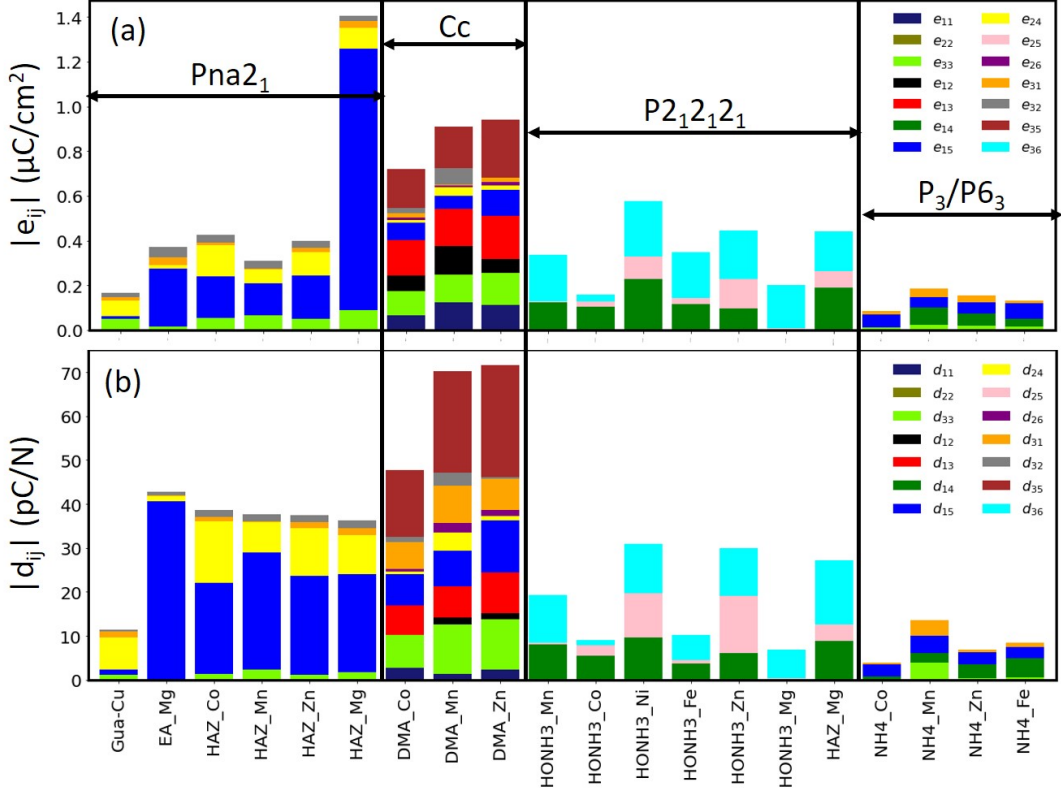


FIG. 4. Comparative view of the components of the (a) piezoelectric stress and (b) piezoelectric strain tensors

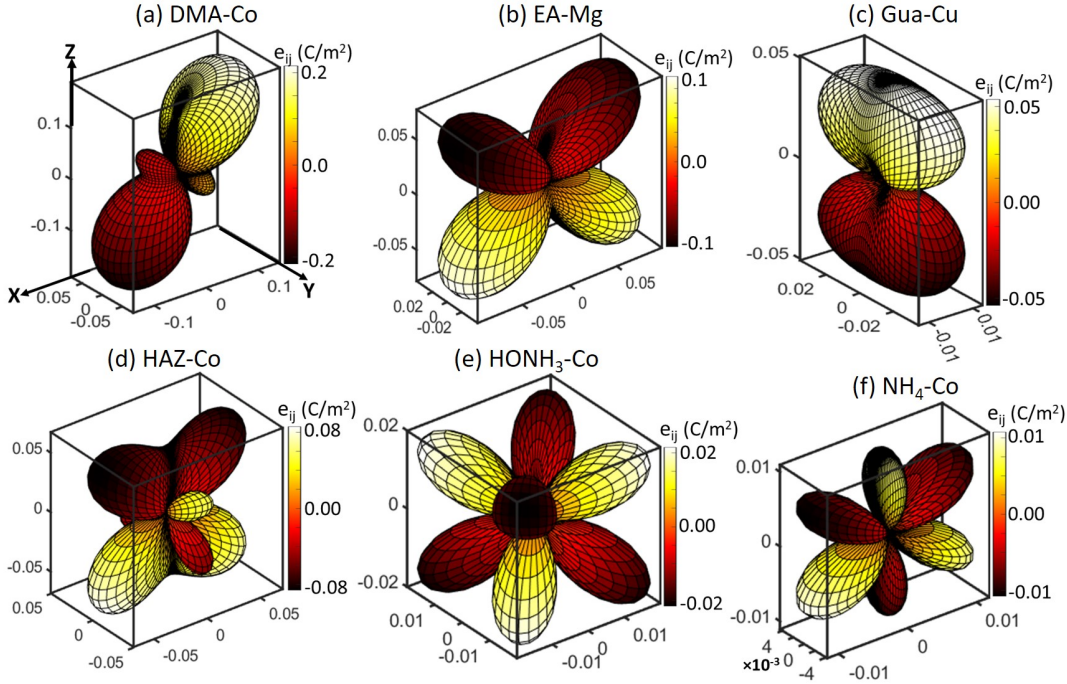


FIG. 5. Piezoelectric stress surface for a representative from each family, as indicated in the titles.

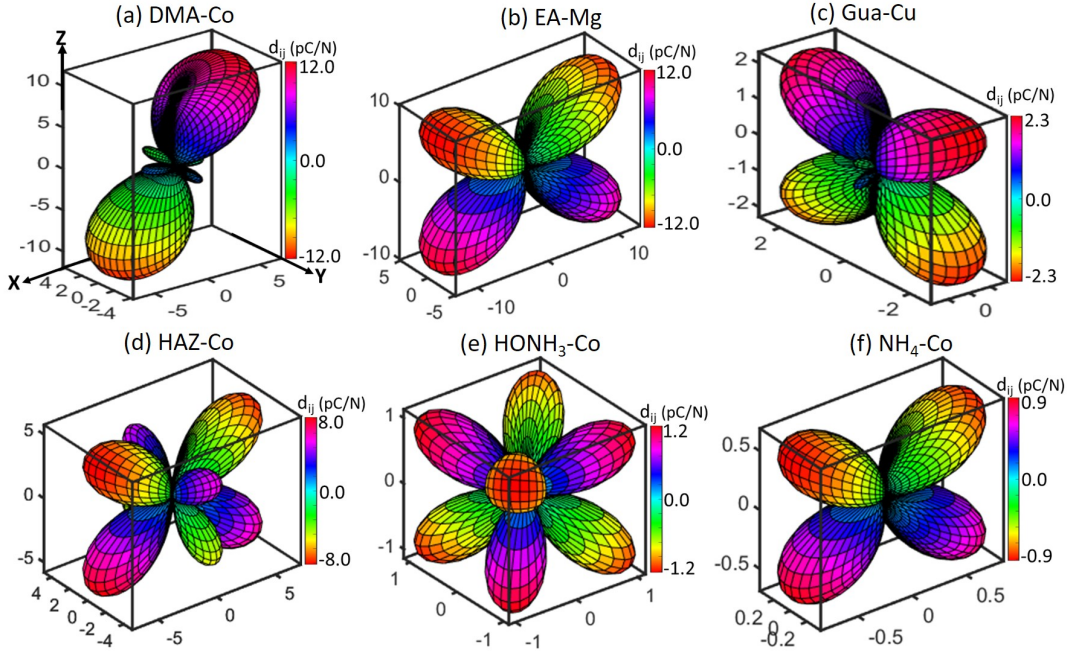


FIG. 6. Piezoelectric strain surface for a representative from each family, as indicated in the titles.

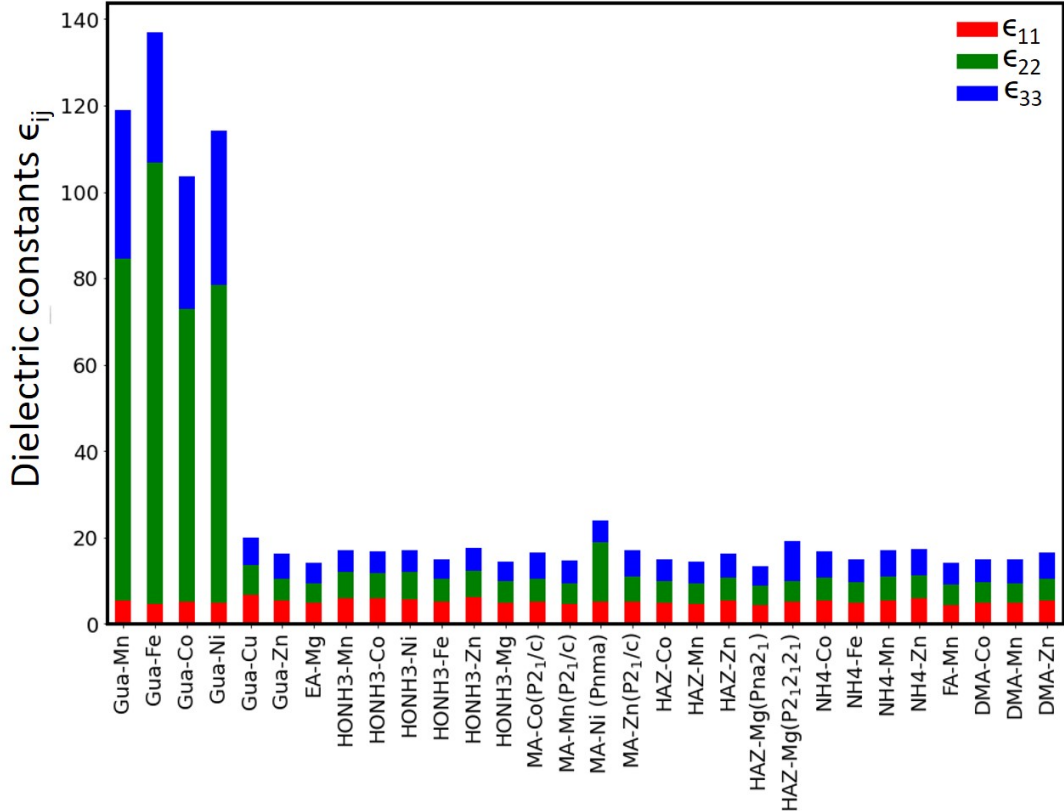


FIG. 7. Comparative view of the components of the dielectric tensor.

TABLE VI. Piezoelectric stress constants e_{ij} in C/m². Materials which do not have experimentally reported structure are underscored.

	e_{15}	e_{24}	e_{31}	e_{32}	e_{33}					
Gua-Cu	-0.011	0.069	-0.017	0.018	0.051					
EA-Mg	<u>e_{15}</u> -0.261	<u>e_{24}</u> -0.014	<u>e_{31}</u> -0.035	<u>e_{32}</u> -0.045	<u>e_{33}</u> -0.015					
DMA-Co	0.065	0.071	0.160	0.077	0.012	-0.009	-0.020	0.025	0.107	0.175
DMA-Mn	0.124	0.129	0.165	0.058	0.041	0.006	-0.004	0.073	0.122	0.187
DMA-Zn	0.112	0.062	0.196	0.114	0.019	-0.017	0.020	0.001	0.141	0.258
HONH ₃ -Mn	<u>e_{14}</u> -0.124	<u>e_{25}</u> 0.003	<u>e_{36}</u> -0.211							
HONH ₃ -Co	-0.102	-0.027	-0.031							
HONH ₃ -Ni	-0.226	0.103	0.247							
<u>HONH₃-Fe</u>	-0.065	-0.004	-0.135							
HONH ₃ -Zn	-0.097	-0.130	-0.218							
HONH ₃ -Mg	-0.005	-0.002	-0.193							
HAZ-Co	<u>e_{15}</u> -0.185	<u>e_{24}</u> 0.138	<u>e_{31}</u> -0.012	<u>e_{32}</u> 0.035	<u>e_{33}</u> -0.054					
HAZ-Mn	-0.143	0.060	0.004	0.037	-0.067					
HAZ-Zn	-0.194	0.104	-0.021	0.028	-0.050					
HAZ-Mg (Pna2 ₁)	-1.172	0.090	-0.032	0.022	-0.088					
HAZ-Mg (P2 ₁ 2 ₁ 2 ₁)	<u>e_{14}</u> -0.190	<u>e_{25}</u> -0.074	<u>e_{36}</u> -0.177							
NH ₄ -Co	0.001	-0.057	0.017	0.011						
NH ₄ -Fe	0.078	-0.046	0.037	0.023						
NH ₄ -Zn	0.055	-0.049	0.031	0.019						
NH ₄ -Mn	0.034	-0.069	-0.013	-0.015						

TABLE VII. Piezoelectric stress constants d_{ij} in pC/N. Materials which do not have experimentally reported structure are underscored.

	d_{15}	d_{24}	d_{31}	d_{32}	d_{33}					
Gua-Cu	-1.05	7.36	-1.41	0.39	1.23					
EA-Mg	<u>d_{15}</u> -40.55	<u>d_{24}</u> -1.24	<u>d_{31}</u> -0.14	<u>d_{32}</u> -0.84	<u>d_{33}</u> 0.01					
DMA-Co	-2.77	0.18	6.52	7.21	0.59	-0.57	-6.19	1.19	7.37	15.05
DMA-Mn	-1.29	1.58	7.11	8.16	4.04	2.19	-8.56	2.81	11.29	23.16
DMA-Zn	-2.34	-1.39	9.15	11.85	1.05	-1.32	-7.10	-0.50	11.46	25.36
HONH ₃ -Mn	<u>d_{14}</u> -8.06	<u>d_{25}</u> 0.33	<u>d_{36}</u> -11.01							
HONH ₃ -Co	-5.47	-2.35	-1.25							
HONH ₃ -Ni	-9.65	9.97	11.38							
<u>HONH₃-Fe</u>	-3.66	-0.75	-5.85							
HONH ₃ -Zn	-6.03	-13.16	-10.86							
HONH ₃ -Mg	-0.22	-0.16	-6.47							
HAZ-Co	<u>d_{15}</u> -20.73	<u>d_{24}</u> 14.08	<u>d_{31}</u> -1.01	<u>d_{32}</u> 1.54	<u>d_{33}</u> -1.32					
HAZ-Mn	-26.72	6.90	-0.07	1.71	-2.33					
HAZ-Zn	-22.48	10.71	-1.41	1.62	-1.24					
HAZ-Mg (Pna2 ₁)	-22.40	8.86	-1.53	1.73	-1.74					
HAZ-Mg (P2 ₁ 2 ₁ 2 ₁)	<u>d_{14}</u> -8.91	<u>d_{25}</u> -3.62	<u>d_{36}</u> -14.64							
NH ₄ -Co	0.49	-2.90	0.37	-0.20						
NH ₄ -Mn	1.99	-4.09	-3.55	4.00						
NH ₄ -Zn	3.07	-2.73	0.71	-0.42						
NH ₄ -Fe	4.30	-2.47	1.05	-0.63						

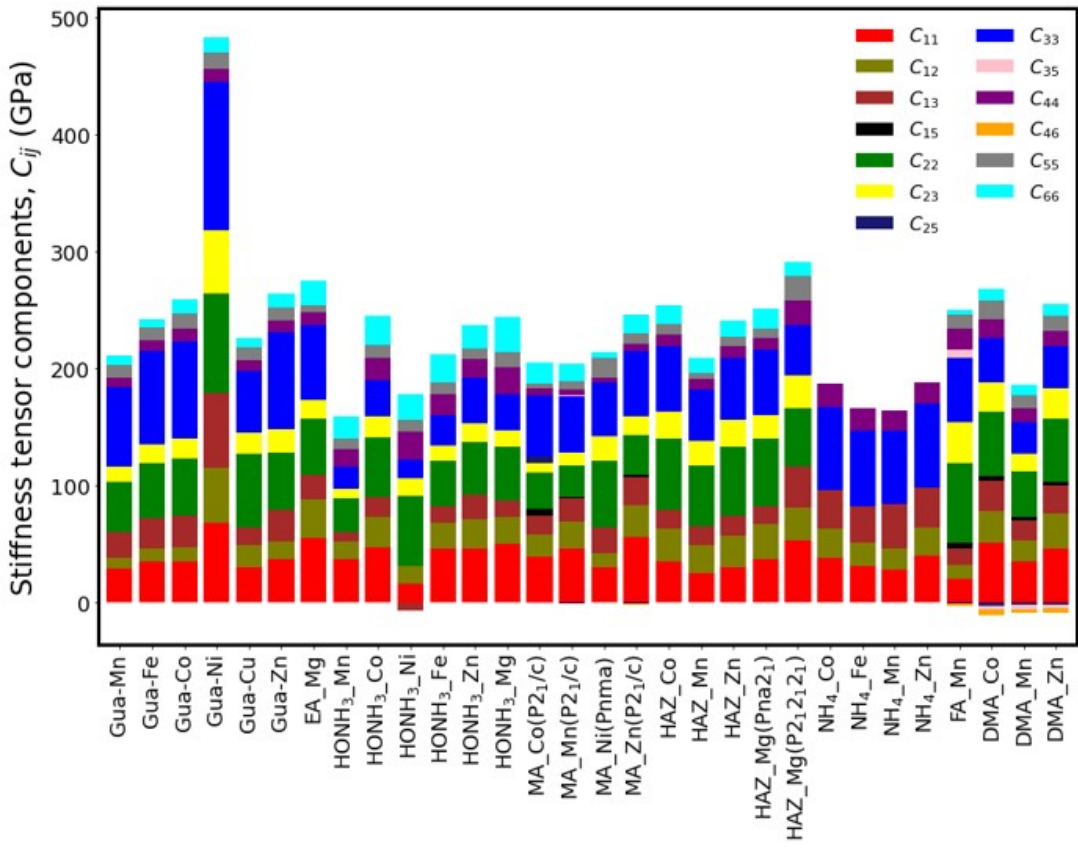


FIG. 8. Comparative view of the components of the stiffness tensor (C_{ij}).

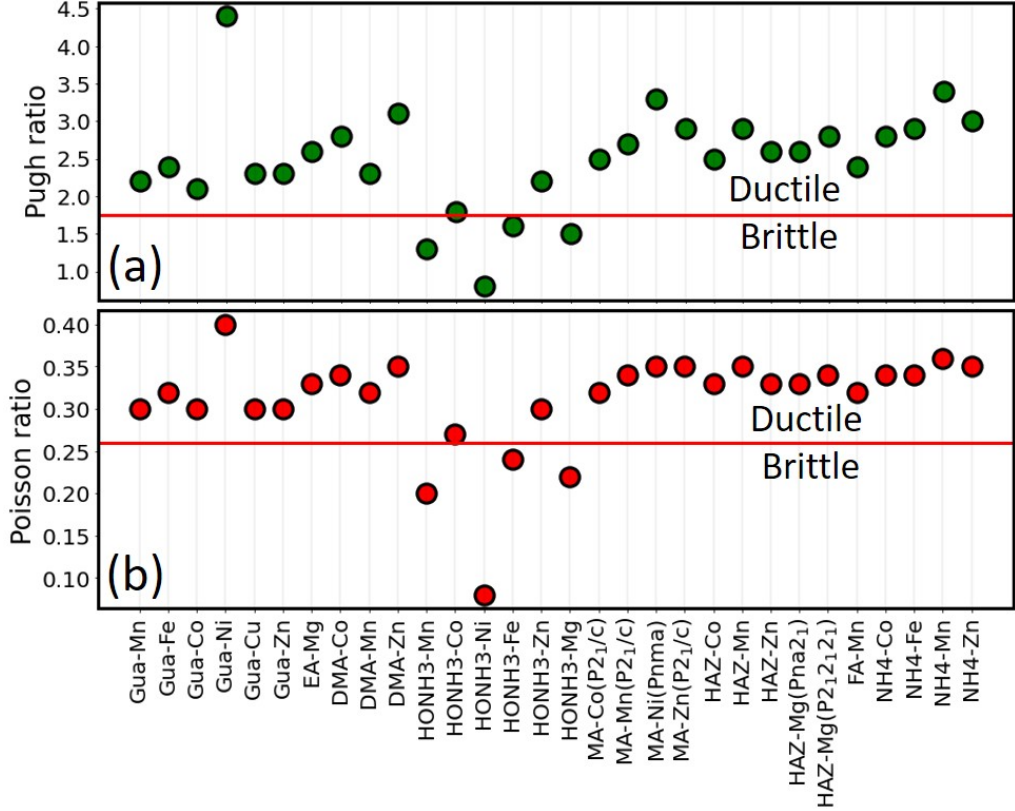


FIG. 9. Pugh (a) and Poisson (b) ratios of formates studied in this work.

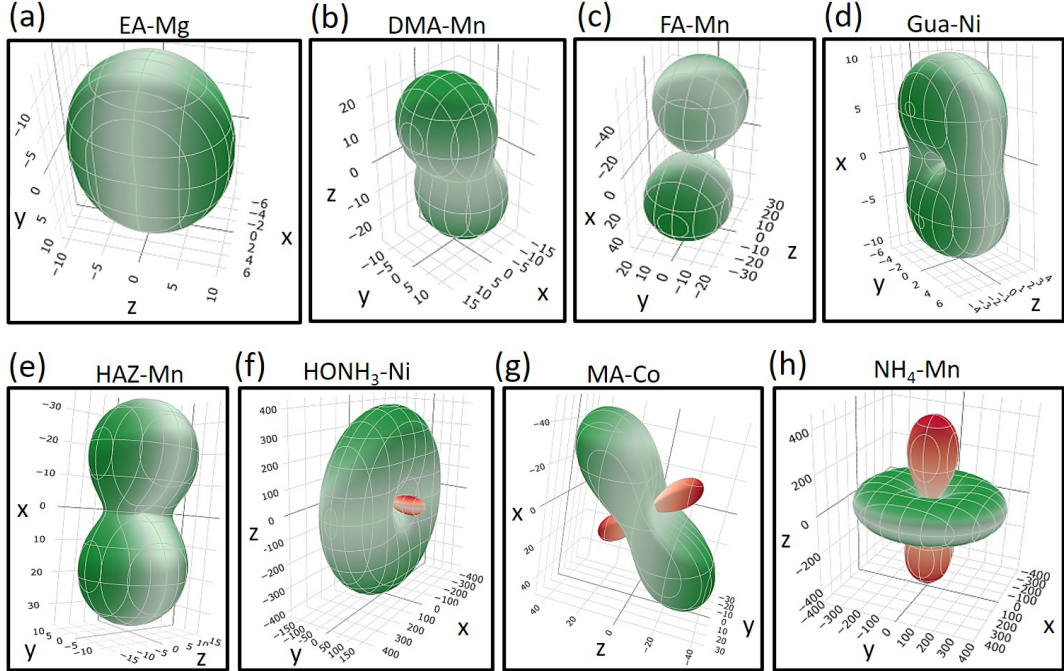


FIG. 10. 3D plots of linear compressibility for a representative material in each family as given in the titles. Green and red colors correspond to positive and negative values, respectively.

TABLE VIII. Components of stiffness tensor C_{ij} in GPa. Materials which do not have experimentally reported structure are underscored.

	C_{11}	C_{12}	C_{13}	C_{22}	C_{23}	C_{33}	C_{44}	C_{55}	C_{66}
Gua-Mn	28.6	9.5	22.3	42.6	13.2	68.2	7.94	10.6	8.3
Gua-Fe	34.6	11.2	26.5	46.9	15.3	80.0	9.3	11.6	6.4
Gua-Co	34.5	12.3	26.7	49.9	17.0	82.9	10.3	13.0	11.9
Gua-Ni	68.4	46.7	64.2	84.6	53.6	127.0	11.0	14.4	13.0
Gua-Cu	29.7	19.7	14.3	63.6	17.4	52.8	9.4	10.6	8.9
Gua-Zn	36.6	15.3	27.0	49.4	19.5	83.1	10.3	10.9	12.0
	C_{11}	C_{12}	C_{13}	C_{22}	C_{23}	C_{33}	C_{44}	C_{55}	C_{66}
EA-Mg	55.3	32.3	20.9	48.5	15.9	63.6	11.2	6.4	21.2
	C_{11}	C_{12}	C_{13}	C_{15}	C_{22}	C_{23}	C_{25}	C_{33}	C_{35}
DMA-Co	50.6	27.7	25.2	4.9	54.8	24.8	-3.4	37.8	-3.0
DMA-Mn	34.9	18.3	17.1	2.2	39.6	15.2	-2.3	26.7	-3.3
DMA-Zn	46.4	29.2	24.2	3.4	54.2	25.4	-2.2	35.7	-3.3
	C_{11}	C_{12}	C_{13}	C_{22}	C_{23}	C_{33}	C_{44}	C_{55}	C_{66}
HONH ₃ -Mn	36.9	15.2	7.8	29.3	8.0	18.6	15.4	9.0	19.2
HONH ₃ -Co	46.9	25.6	17.9	50.9	18.0	31.1	18.6	11.3	25.0
HONH ₃ -Ni	16.1	15.0	-6.6	59.8	15.3	16.1	23.4	10.4	21.7
HONH ₃ -Fe	46.0	21.8	13.7	39.1	12.9	26.2	17.9	10.8	23.1
HONH ₃ -Zn	45.6	25.1	21.4	44.8	16.5	38.4	16.0	9.0	20.1
HONH ₃ -Mg	50.2	22.5	14.2	45.6	14.4	31.2	23.2	12.6	29.8
	C_{11}	C_{12}	C_{13}	C_{22}	C_{23}	C_{33}	C_{44}	C_{55}	C_{66}
MA-Ni (Pnma)	29.7	12.2	22.2	56.7	21.2	46.3	3.6	17.3	4.9
	C_{11}	C_{12}	C_{13}	C_{15}	C_{22}	C_{23}	C_{25}	C_{33}	C_{35}
MA-Co (P2 ₁ /c)	39.1	18.6	16.3	6.0	30.8	8.6	5.2	52.1	-0.8
MA-Zn (P2 ₁ /c)	55.9	27.1	24.3	1.8	33.8	16.4	-1.4	55.2	0.6
MA-Mn (P2 ₁ /c)	46.4	22.7	19.7	1.3	26.4	11.6	-1.2	47.8	0.8
	C_{11}	C_{12}	C_{13}	C_{22}	C_{23}	C_{33}	C_{44}	C_{55}	C_{66}
HAZ-Co	35.0	28.4	15.2	61.2	23.3	56.0	9.8	9.0	15.8
HAZ-Mn	25.0	24.4	15.5	52.0	21.5	43.9	8.7	5.3	13.0
HAZ-Zn	30.4	26.6	16.7	58.8	23.9	52.4	9.7	8.7	13.7
HAZ-Mg (Pna2 ₁)	36.8	29.7	15.3	58.3	19.5	56.6	10.1	7.7	16.9
HAZ-Mg (P2 ₁ 2 ₁ 2 ₁)	53.3	28.0	35.1	49.1	28.5	42.7	21.3	20.5	12.1
	C_{11}	C_{12}	C_{13}	C_{15}	C_{22}	C_{23}	C_{25}	C_{33}	C_{35}
FA-Mn	19.6	11.9	14.1	5.7	67.2	35.8	-0.9	54.4	7.1
	C_{11}	C_{12}	C_{13}	C_{33}	C_{44}				
NH ₄ -Co	38.4	24.1	33.2	71.5	20.2				
NH ₄ -Fe	30.8	20.6	30.4	65.6	18.1				
NH ₄ -Mn	28.3	17.7	37.7	63.1	17.0				
NH ₄ -Zn	39.9	24.2	34.3	71.4	18.0				

TABLE IX. Dielectric constants. Materials which do not have experimentally reported structure are underscored.

	ϵ_{11}	ϵ_{22}	ϵ_{33}			
Gua-Mn	5.31	79.19	34.42			
Gua-Fe	4.62	102.12	30.26			
Gua-Co	5.26	67.72	30.55			
Gua-Ni	4.94	73.59	35.51			
Gua-Cu	6.79	6.85	6.26			
Gua-Zn	5.33	5.20	5.68			
EA-Mg	4.82	4.63	4.67			
DMA-Co	4.92	4.61	5.35	0.33	Expt	Ref.
DMA-Mn	4.93	4.53	5.53	0.41	3 – 6	[100]
DMA-Zn	5.50	4.98	6.00	0.41	8 – 10	[101]
HONH ₃ -Mn	5.90	6.04	5.21			
HONH ₃ -Co	5.84	5.93	4.95			
HONH ₃ -Ni	5.56	6.48	5.08			
HONH ₃ -Fe	5.14	5.29	4.46			
HONH ₃ -Zn	6.26	6.04	5.15			
HONH ₃ -Mg	4.84	5.01	4.43			
MA-Co (P2 ₁ /c)	5.21	5.34	5.89	0.22		
MA-Zn (P2 ₁ /c)	5.17	5.83	6.06	-0.20		
MA-Mn (P2 ₁ /c)	4.62	4.85	5.29	-0.13		
MA-Ni (Pnma)	5.21	13.69	5.11			
HAZ-Co	4.87	5.05	5.03			
HAZ-Mn	4.66	4.84	4.83			
HAZ-Zn	5.30	5.41	5.49			
HAZ-Mg (Pna2 ₁)	4.31	4.65	4.50			
HAZ-Mg (P2 ₁ 2 ₁ 2 ₁)	5.17	4.75	9.29			
FA-Mn	4.36	4.72	5.07	0.27		
NH ₄ -Co	5.38	5.38	6.04			
NH ₄ -Fe	4.77	4.77	5.28			
NH ₄ -Mn	5.51	5.51	5.94			
NH ₄ -Zn	5.28	5.28	6.17			

Zn) formates is different from the low temperature phase reported experimentally, which suggests additional phase transitions at very low temperatures. The spontaneous polarizations range from 0.2 to 7.8 $\mu\text{C}/\text{cm}^2$ with the largest values being in DMA-M family. They are expected to be reversible by the electric field as the upper estimate for the energy barrier is 200 meV/atom. We also find polarization values often exceeding experimentally reported ones, which we attribute to the difference in the direction of measurement. Thus, our study could guide towards optimization of materials performance. Typical dielectric constants are typically 5.0. Nevertheless, Gua family exhibits outstandingly large values in range 4.6 – 102.1, which, however, need to be further validated. Intrinsic piezoelectric strain and stress constants are in the range 0.1 – 25.8 $\mu\text{C}/\text{cm}^2$ and 0.1 – 26.7 pC/N, respectively. The responses were also found to be highly anisotropic. Components of elastic stiffness tensor range

from 0.3 to 127.0 GPa. On the basis of Pugh and Poisson ratio we found most of the materials to be ductile. Computations predict that linear compressibility is highly anisotropic and many materials (e.g. HONH₃-Ni, NH₄-Mn, Gua-Ni and MA-Co) exhibit either zero or even negative values. All computational data are available from Ref. [76].

Our study reveals that additional investigations are needed to validate and explain outstanding dielectric response of Gua-M formates, and large piezoelectric response of DMA-M formates, along with the large negative compressibility values for HONH₃-Ni and NH₄-Mn. Investigation on the origin of negative and/or nearly zero values of compressibility is also required.

TABLE X. Mechanical properties of formates. B , E and G are average bulk, Young and shear moduli of bulk polycrystal, respectively. B/G , ν , CP and LC_{min} are Pugh's ratio, Poisson's ratio, Cauchy's pressure and minimum linear compressibility, respectively. Materials which do not have experimentally reported structure are underscored.

	B (GPa)	E (GPa)	G (GPa)	B/G	ν	CP (GPa)	LC_{min} (TPa $^{-1}$)
Gua-Mn	23.5	28.2	10.8	2.2	0.30	1.5	2.41
Gua-Fe	27.4	30.2	11.5	2.4	0.32	1.9	2.18
Gua-Co	29.0	35.7	13.8	2.1	0.30	2.0	2.45
Gua-Ni	64.1	40.7	14.6	4.4	0.4	35.6	0.05
Gua-Cu	26.1	30.0	11.4	2.3	0.3	10.4	5.03
Gua-Zn	30.3	34.2	13.0	2.3	0.3	5.0	2.46
EA-Mg	33.7	34.2	12.9	2.6	0.33	21.1	6.72
DMA-Co	32.5	31.3	11.7	2.8	0.34	11.4	6.85
DMA-Mn	20.9	23.8	9.0	2.3	0.32	6.3	8.51
DMA-Zn	31.7	28.2	10.4	3.1	0.35	15.3	5.36
HONH ₃ -Mn	15.3	27.5	11.5	1.3	0.20	-0.2	11.33
HONH ₃ -Co	26.8	36.9	14.5	1.8	0.27	7.0	7.18
HONH ₃ -Ni	8.5	21.7	10.1	0.8	0.08	-8.4	-188.08
HONH ₃ -Fe	22.0	34.0	13.6	1.6	0.24	3.9	7.63
HONH ₃ -Zn	28.0	33.8	13.0	2.2	0.30	9.1	7.51
HONH ₃ -Mg	24.5	41.2	16.9	1.5	0.22	-0.7	8.72
MA-Co (P2 ₁ /c)	19.9	21.1	8.0	2.5	0.32	12.4	-32.24
MA-Mn (P2 ₁ /c)	23.7	23.4	8.8	2.7	0.34	17.8	-0.15
MA-Ni (Pnma)	27.8	23.1	8.5	3.3	0.35	8.6	1.96
MA-Zn (P2 ₁ /c)	29.7	27.5	10.2	2.9	0.35	20.9	4.22
HAZ-Co	30.1	31.5	11.9	2.5	0.33	18.6	1.77
HAZ-Mn	24.8	23.1	8.6	2.9	0.35	15.6	-1.73
HAZ-Zn	28.6	28.8	10.8	2.6	0.33	16.9	0.82
HAZ-Mg (Pna2 ₁)	30.2	31.3	11.8	2.6	0.33	19.6	3.28
HAZ-Mg (P2 ₁ 2 ₁ 2 ₁)	36.2	34.7	12.9	2.8	0.34	6.6	5.28
FA-Mn	22.8	25.4	9.6	2.4	0.32	-6.1	1.07
NH ₄ -Co	33.9	32.0	11.9	2.8	0.34	3.9	-1.73
NH ₄ -Fe	29.5	27.8	10.3	2.9	0.34	2.5	-4.50
NH ₄ -Mn	18.5	15.1	5.5	3.4	0.36	0.7	-439.63
NH ₄ -Zn	34.7	31.5	11.7	3.0	0.35	6.2	-2.04

IV. ACKNOWLEDGMENT

The work is supported by the National Science Foundation under the grant EPMD-2029800.

V. DATA AVAILABILITY

The data that support the findings of this study are available from our github repository[76] as well as from the corresponding author upon reasonable request.

VI. REFERENCES

- [1] W. Li, A. Stroppa, Z. Wang, and S. Gao, *Hybrid Organic-Inorganic Perovskites* (2020).
- [2] Y. Ma and Y. Sun, *Journal of Applied Physics* **127**, 080901 (2020).
- [3] R. Shang, G.-C. Xu, Z.-M. Wang, and S. Gao, *Chemistry – A European Journal* **20**, 1146 (2014).
- [4] R. Shang, S. Chen, B.-W. Wang, Z.-M. Wang, and S. Gao, *Angewandte Chemie International Edition* **55**, 2097 (2016).
- [5] M. Ptak, M. Maczka, A. Gagor, A. Sieradzki, A. Stroppa, D. Di Sante, J. M. Perez-Mato, and L. Macalik, *Dalton Trans.* **45**, 2574 (2016).
- [6] M. Ptak, M. Maczka, A. Gagor, A. Sieradzki, B. Bondzior, P. Deren, and S. Pawlus, *Phys. Chem. Chem. Phys.* **18**, 29629 (2016).
- [7] Y. Imai, B. Zhou, Y. Ito, H. Fijimori, A. Kobayashi, Z.-M. Wang, and H. Kobayashi, *Chem Asian J* **7**, 2786 (2012).
- [8] B. Zhou, Y. Imai, A. Kobayashi, Z.-M. Wang, and H. Kobayashi, *Angew Chem Int Ed Engl* **50**, 11441 (2011).

- [9] T. Asaji, Y. Ito, J. Seliger, V. Zagar, A. Gradisek, and T. Apih, *The Journal of Physical Chemistry A* **116**, 12422 (2012).
- [10] V. V. Shvartsman and D. C. Lupascu, *Journal of the American Ceramic Society* **95**, 1 (2012).
- [11] K. Asadi and M. A. van der Veen, *European Journal of Inorganic Chemistry* **2016**, 4332 (2016).
- [12] P. Jain, V. Ramachandran, R. J. Clark, H. D. Zhou, B. H. Toby, N. S. Dalal, H. W. Kroto, and A. K. Cheetham, *Journal of the American Chemical Society* **131**, 13625 (2009).
- [13] P. Jain, N. S. Dalal, B. H. Toby, H. W. Kroto, and A. K. Cheetham, *Journal of the American Chemical Society* **130**, 10450 (2008).
- [14] D.-W. Fu, W. Zhang, H.-L. Cai, Y. Zhang, J.-Z. Ge, R.-G. Xiong, S. Huang, and T. Nakamura, *Angewandte Chemie (International ed. in English)* **50**, 11947 (2011).
- [15] D. Di Sante, A. Stroppa, P. Jain, and S. Picozzi, *Journal of the American Chemical Society* **135**, 18126 (2013).
- [16] L. Hu, Z. Wang, H. Wang, Z. Qu, and Q. Chen, *RSC Adv.* **8**, 13675 (2018).
- [17] W. Wang, L.-Q. Yan, J.-Z. Cong, Y.-L. Zhao, F. Wang, S.-P. Shen, T. Zou, D. Zhang, S.-G. Wang, X.-F. Han, and Y. Sun, *Scientific reports* **3**, 2024 (2013).
- [18] C. Liu, K. Zhai, Z. Yu, A. Nie, Z. Liu, and Y. Sun, *The Journal of Physical Chemistry C* **124**, 16111 (2020).
- [19] Y. Ma, J. Cong, Y. Chai, L. Yan, D. Shang, and Y. Sun, *Applied Physics Letters* **111**, 042901 (2017).
- [20] Y. Ma, J. Cong, and Y. Sun, *Journal of Physics: Condensed Matter* **31**, 205701 (2019).
- [21] Z. Yu, C. Liu, Z. Shen, K. Zhai, D. Xu, A. Nie, J. Xiang, F. Wen, C. Mu, B. Wang, L. Wang, L. Wang, Z. Liu, and Y. Tian, *The Journal of Physical Chemistry Letters* **11**, 9566 (2020).
- [22] M. Simenas, S. Balciunas, M. Maczka, J. Banys, and E. E. Tornau, *Phys. Chem. Chem. Phys.* **18**, 18528 (2016).
- [23] G.-C. Xu, W. Zhang, X.-M. Ma, Y.-H. Chen, L. Zhang, H.-L. Cai, Z.-M. Wang, R.-G. Xiong, and S. Gao, *Journal of the American Chemical Society* **133**, 14948 (2011).
- [24] M. Maczka, A. Pietraszko, B. Macalik, and K. Hermanowicz, *Inorganic Chemistry* **53**, 787 (2014).
- [25] I. E. Collings, M. Bykov, E. Bykova, M. G. Tucker, S. Petitgirard, M. Hanfland, K. Glazyrin, S. van Smaalen, A. L. Goodwin, L. Dubrovinsky, and N. Dubrovinskaia, *CrystEngComm* **18**, 8849 (2016).
- [26] G.-C. Xu, X.-M. Ma, L. Zhang, Z.-M. Wang, and S. Gao, *Journal of the American Chemical Society* **132**, 9588 (2010).
- [27] Y. Sun, Z. Zhuo, and X. Wu, *RSC Advances* **6**, 113234 (2016).
- [28] M. Maczka, A. Gagor, M. Ptak, W. Paraguassu, T. A. da Silva, A. Sieradzki, and A. Pikul, *Chemistry of Materials* **29**, 2264 (2017).
- [29] S. Chen, R. Shang, K.-L. Hu, Z.-M. Wang, and S. Gao, *Inorg. Chem. Front.* **1**, 83 (2014).
- [30] K. L. Svane and A. Walsh, *The Journal of Physical Chemistry C* **121**, 421 (2017).
- [31] A. Stroppa, P. Barone, P. Jain, J. M. Perez-Mato, and S. Picozzi, *Advanced materials (Weinheim)* **25**, 2284 (2013).
- [32] P. C. Rout and V. Srinivasan, *Phys. Rev. Materials* **2**, 014407 (2018).
- [33] Y. Tian, A. Stroppa, Y.-S. Chai, P. Barone, M. Perez-Mato, S. Picozzi, and Y. Sun, *Physica Status Solidi Rapid Research Letters* **9**, 62 (2015).
- [34] A. Stroppa, P. Jain, P. Barone, M. Marsman, J. M. Perez-Mato, A. Cheetham, H. Kroto, and S. Picozzi, *Angewandte Chemie (International ed. in English)* **50**, 5847 (2011).
- [35] J.-C. Tan, P. Jain, and A. K. Cheetham, *Dalton Trans.* **41**, 3949 (2012).
- [36] P. S. Ghosh and I. Ponomareva, *J. Phys. Chem. Lett.* **12**, 7560 (2021), <https://doi.org/10.1021/acs.jpclett.1c02156>.
- [37] P. S. Ghosh and I. Ponomareva, *The Journal of Physical Chemistry Letters* **13**, 3143 (2022), <https://doi.org/10.1021/acs.jpclett.2c00288>.
- [38] W. Li, M. R. Probert, M. Kosa, T. D. Bennett, A. Thirumurugan, R. P. Burwood, M. Parinello, J. A. K. Howard, and A. K. Cheetham, *Journal of the American Chemical Society* **134**, 11940 (2012).
- [39] A. B. Cairns and A. L. Goodwin, *Phys. Chem. Chem. Phys.* **17**, 20449 (2015).
- [40] D. Gui, L. Ji, A. Muhammad, W. Li, W. Cai, Y. Li, X. Li, X. Wu, and P. Lu, *The Journal of Physical Chemistry Letters* **9**, 751 (2018).
- [41] W. Li, A. Thirumurugan, P. T. Barton, Z. Lin, S. Henke, H. H.-M. Yeung, M. T. Wharmby, E. G. Bithell, C. J. Howard, and A. K. Cheetham, *Journal of the American Chemical Society* **136**, 7801 (2014).
- [42] G. Kieslich, A. C. Forse, S. Sun, K. T. Butler, S. Kumagai, Y. Wu, M. R. Warren, A. Walsh, C. P. Grey, and A. K. Cheetham, *Chemistry of Materials* **28**, 312 (2016).
- [43] S. A. LoCicero, C. M. Averback, U. Shumnyk, E. S. Choi, and D. R. Talham, *The Journal of Physical Chemistry C* **124**, 21113 (2020).
- [44] W. Li, Z. Wang, F. Deschler, S. Gao, R. H. Friend, and A. K. Cheetham, *Nature Reviews Materials* **2**, 16099 (2017).
- [45] Z. Wang, K. Hu, S. Gao, and H. Kobayashi, *Advanced materials* **22**, 1526 (2010).
- [46] K.-L. Hu, M. Kurmoo, Z. Wang, and S. Gao, *Chemistry – A European Journal* **15**, 12050 (2009).
- [47] C. Liu, K. Zhai, Z. Yu, A. Nie, Z. Liu, and Y. Sun, *The Journal of Physical Chemistry C* **124**, 16111 (2020).
- [48] R. Shang, X. Sun, Z.-M. Wang, and S. Gao, *Chemistry – An Asian Journal* **7**, 1697 (2012).
- [49] L. Mazzuca, L. Cañadillas-Delgado, O. Fabelo, J. A. Rodríguez-Velamazán, J. Luzón, O. Vallcorba, V. Simonet, C. V. Colin, and J. Rodríguez-Carvajal, *Chemistry – A European Journal* **24**, 388 (2018).
- [50] B. Pato-Doldán, L. C. Gómez-Aguirre, A. P. Hansen, J. Mira, S. Castro-García, M. Sánchez-Andújar, M. A. Señaris-Rodríguez, V. S. Zapf, and J. Singleton, *J. Mater. Chem. C* **4**, 11164 (2016).
- [51] B. Liu, R. Shang, K.-L. Hu, Z.-M. Wang, and S. Gao, *Inorganic Chemistry* **51**, 13363 (2012).
- [52] M. Maczka, A. Ciupa, A. Gagor, A. Sieradzki, A. Pikul, B. Macalik, and M. Drozd, *Inorganic Chemistry* **53**, 5260 (2014).
- [53] W. D. C. B. Gunatilleke, K. Wei, Z. Niu, L. Wojtas, G. Nolas, and S. Ma, *Dalton Trans.* **46**, 13342 (2017).

- [54] I. E. Collings, J. A. Hill, A. B. Cairns, R. I. Cooper, A. L. Thompson, J. E. Parker, C. C. Tang, and A. L. Goodwin, *Dalton Trans.* **45**, 4169 (2016).
- [55] T. Asaji, Y. Ito, H. Fujimori, and B. Zhou, *The Journal of Physical Chemistry C* **123**, 4291 (2019), <https://doi.org/10.1021/acs.jpcc.8b11789>.
- [56] P. Peksa, J. K. Zareba, M. Ptak, M. Maczka, A. Gagor, S. Pawlus, and A. Sieradzki, *The Journal of Physical Chemistry C* **124**, 18714 (2020), <https://doi.org/10.1021/acs.jpcc.0c06141>.
- [57] R. Shang, G.-C. Xu, Z.-M. Wang, and S. Gao, *Chemistry – A European Journal* **20**, 1146 (2014).
- [58] G. Kresse and J. Hafner, *Phys. Rev. B* **47**, 558 (1993).
- [59] G. Kresse and J. Furthmüller, *Comput. Mater. Sci.* **6**, 15 (1996).
- [60] G. Kresse and J. Furthmüller, *Phys. Rev. B* **54**, 11169 (1996).
- [61] G. Kresse and D. Joubert, *Phys. Rev. B* **59**, 1758 (1999).
- [62] J. P. Perdew, K. Burke, and M. Ernzerhof, *Phys. Rev. Lett.* **77**, 3865 (1996).
- [63] S. Grimme, *J. Comput. Chem.* **27**, 1787 (2006).
- [64] S. Grimme, J. Antony, S. Ehrlich, and H. Krieg, *J. Chem. Phys.* **132**, 154104 (2010).
- [65] P. S. Ghosh, J. Doherty, S. Lisenkov, and I. Ponomareva, *J. Phys. Chem. C* **125**, 16296 (2021), <https://doi.org/10.1021/acs.jpcc.1c03980>.
- [66] P. S. Ghosh, D. DeTellem, J. Ren, S. Witanachchi, S. Ma, S. Lisenkov, and I. Ponomareva, *Phys. Rev. Lett.* **128**, 077601 (2022).
- [67] P. S. Ghosh, S. Lisenkov, and I. Ponomareva, *Phys. Rev. Lett.* **125**, 207601 (2020).
- [68] M. Kingsland, P. S. Ghosh, S. Lisenkov, and I. Ponomareva, *The Journal of Physical Chemistry C* **125**, 8794 (2021), <https://doi.org/10.1021/acs.jpcc.1c01138>.
- [69] R. Kashikar, P. S. Ghosh, S. Lisenkov, B. R. K. Nanda, and I. Ponomareva, *Phys. Rev. B* **104**, 235132 (2021).
- [70] P. E. Blöchl, *Phys. Rev. B* **50**, 17953 (1994).
- [71] S. L. Dudarev, G. A. Botton, S. Y. Savrasov, C. J. Humphreys, and A. P. Sutton, *Phys. Rev. B* **57**, 1505 (1998).
- [72] R. D. King-Smith and D. Vanderbilt, *Phys. Rev. B* **47**, 1651 (1993).
- [73] D. Vanderbilt and R. D. King-Smith, *Phys. Rev. B* **48**, 4442 (1993).
- [74] Y. Le Page and P. Saxe, *Phys. Rev. B* **65**, 104104 (2002).
- [75] M. Cococcioni and S. de Gironcoli, *Phys. Rev. B* **71**, 035105 (2005).
- [76] “Hybrid-formate-perovskites,” <https://github.com/USFmatscilib/Hybrid-Formate-Perovskites> (2023).
- [77] P. Jain, N. S. Dalal, B. H. Toby, H. W. Kroto, and A. K. Cheetham, *Journal of the American Chemical Society* **130**, 10450 (2008).
- [78] G. Kieslich, S. Kumagai, K. T. Butler, T. Okamura, C. H. Hendon, S. Sun, M. Yamashita, A. Walsh, and A. K. Cheetham, *Chem. Commun.* **51**, 15538 (2015).
- [79] P. S. Ghosh, D. DeTellem, J. Ren, S. Witanachchi, S. Ma, S. Lisenkov, and I. Ponomareva, *Phys. Rev. Lett.* **128**, 077601 (2022).
- [80] N. A. Spaldin, *Journal of Solid State Chemistry* **195**, 2 (2012), polar Inorganic Materials: Design Strategies and Functional Properties.
- [81] S. Hu, H. Gao, Y. Qi, Y. Tao, Y. Li, J. R. Reimers, M. Bokdam, C. Franchini, D. Di Sante, A. Stroppa, and W. Ren, *The Journal of Physical Chemistry C* **121**, 23045 (2017), <https://doi.org/10.1021/acs.jpcc.7b05929>.
- [82] C. Capillas, E. S. Tasci, G. de la Flor, D. Orobengoa, J. M. Perez-Mato, and M. I. Aroyo, *Inorganic Chemistry* **49**, 1510 (2010), pMID: 20095567, <https://doi.org/10.1021/ic901872g>.
- [83] C. M. Acosta, A. Fazzio, G. M. Dalpian, and A. Zunger, *Physical Review B* **102**, 144106 (2020).
- [84] T. E. Smidt, S. A. Mack, S. E. Reyes-Lillo, A. Jain, and J. B. Neaton, *Scientific Data* **7**, 2052 (2020).
- [85] D. Mainprice, F. Bachmann, R. Hielscher, H. Schaeben, and G. E. Lloyd, *Geological Society, London, Special Publications* **409**, 223 (2015), <https://www.lyellcollection.org/doi/pdf/10.1144/SP409.2>.
- [86] N. H. Yusoff, R. A. M. Osman, M. S. Idris, K. N. D. K. Muhsen, and N. I. M. Nor, *AIP Conference Proceedings* **2203**, 020038 (2020), <https://aip.scitation.org/doi/pdf/10.1063/1.5142130>.
- [87] M. Born, *Mathematical Proceedings of the Cambridge Philosophical Society* **36**, 160–172 (1940).
- [88] F. Mouhat and F. m. c.-X. Coudert, *Phys. Rev. B* **90**, 224104 (2014).
- [89] V. Wang, N. Xu, J.-C. Liu, G. Tang, and W.-T. Geng, *Computer Physics Communications* **267**, 108033 (2021).
- [90] V. Woldemar, *Lehrbuch Der Kristallphysik (Mit Ausschluss Der Kristalloptik)* (B.G. Teubner, Leipzig, Berlin, 1928) pp. 1–978.
- [91] R. Hill, *Proceedings of the Physical Society. Section A* **65**, 349 (1952).
- [92] A. Reuss, *ZAMM - Journal of Applied Mathematics and Mechanics / Zeitschrift für Angewandte Mathematik und Mechanik* **9**, 49 (1929).
- [93] O. L. Anderson, *Journal of Physics and Chemistry of Solids* **24**, 909 (1963).
- [94] *Intermetallics* **19**, 1275 (2011).
- [95] Y. Tian, B. Xu, and Z. Zhao, *International Journal of Refractory Metals and Hard Materials* **33**, 93 (2012).
- [96] J. Islam and A. K. M. A. Hossain, *RSC Adv.* **10**, 7817 (2020).
- [97] M. S. Hossain, M. M. Haque Babu, T. Saha, M. S. Hossain, J. Podder, M. S. Rana, A. Barik, and P. Rani, *AIP Advances* **11**, 055024 (2021), <https://doi.org/10.1063/5.0048979>.
- [98] M. Viswanathan, *The Journal of Physical Chemistry C* **123**, 6711 (2019), <https://doi.org/10.1021/acs.jpcc.8b11194>.
- [99] J. M. Ogborn, I. E. Collings, S. A. Moggach, A. L. Thompson, and A. L. Goodwin, *Chem. Sci.* **3**, 3011 (2012).
- [100] M. Sánchez-Andújar, S. Presedo, S. Yáñez-Vilar, S. Castro-García, J. Shamir, and M. A. Señarís-Rodríguez, *Inorganic Chemistry* **49**, 1510 (2010), pMID: 20095567, <https://doi.org/10.1021/ic901872g>.
- [101] N. Abhyankar, J. J. Kweon, M. Orio, S. Bertaina, M. Lee, E. S. Choi, R. Fu, and N. S. Dalal, *The Journal of Physical Chemistry C* **121**, 6314 (2017), <https://doi.org/10.1021/acs.jpcc.7b00596>.

Supplementary Material

TABLE S1. Computational details and errors associated with estimation of structural parameters. KEYS: ENCUT = Cut-Off Energy and K_D = k-points Density

	Error-a (%)	Error-b (%)	Error-c (%)	Error-V (%)	ENCUT (eV)	K_D (\AA^{-1})
Gua-Mn	-1.2	-0.6	0.7	-1.1	708	0.33
Gua-Fe	-0.8	-0.6	0.3	-1.1	850	0.27
Gua-Co	-0.6	-0.9	0.9	-0.6	708	0.39
Gua-Ni	-0.2	-0.1	0.9	-0.6	850	0.33
Gua-Cu	-0.2	0.4	-0.7	-0.5	700	0.33
Gua-Zn	-1.0	-0.6	-0.9	0.7	708	0.27
EA-Mg	-0.9	0.0	-0.7	-1.6	700	0.42
DMA-Mn	0.0	0.9	-0.2	0.6	700	0.33
HONH ₃ -Mn	-0.1	1.0	-0.8	0.0	850	0.28
HONH ₃ -Co	-0.1	0.8	-0.2	0.5	850	0.28
HONH ₃ -Ni	-0.4	2.6	0.5	2.7	850	0.29
HONH ₃ -Zn	-0.6	1.2	1.2	1.9	850	0.57
HONH ₃ -Mg	-0.3	1.3	-1.0	0.0	708	0.29
MA-Co(Pnma)	-1.2	0.0	1.6	0.4	708	0.34
MA-Co(P21/c)	0.9	0.2	0.6	1.6	708	0.34
MA-Mn	-3.3	-0.2	3.1	-0.5	708	0.34
MA-Ni	-0.4	0.9	2.0	2.5	708	0.34
MA-Zn(Pnma)	-1.2	-0.2	0.9	-0.5	708	0.28
FA-Mn	-2.4	2.1	-2.1	-2.5	700	0.33
HAZ-Co	-0.2	-0.3	-0.8	-1.3	700	0.40
HAZ-Mn	0.7	0.1	-0.3	0.5	700	0.34
HAZ-Zn	-0.1	0.4	0.1	0.3	700	0.35
HAZ-Mg (P2 ₁ 2 ₁ 2 ₁)	1.4	1.1	-1.4	1.1	700	0.40
NH ₄ -Co	-0.4	0-0.4	0.2	0.5	850	0.22
NH ₄ -Fe	-0.3	-0.3	2.5	1.9	850	0.19
NH ₄ -Mn	-0.9	-0.9	2.0	0.0	850	0.22
NH ₄ -Zn	-0.2	-0.2	2.2	1.7	708	0.22

TABLE S2. Mechanical properties of formates. B , E and G are average bulk, Young and shear moduli of bulk polycrystal, respectively. B/G , ν , CP and LC_{min} are Pugh's ratio, Poisson's ratio, Cauchy's pressure and minimum linear compressibility, respectively. Materials which do not have experimentally reported structure are underscored.

	B(GPa)	E(GPa)	G(GPa)	B/G	ν	CP(GPa)	ALC	$LC_{min}(\text{TPa}^{-1})$	$LC_{max}(\text{TPa}^{-1})$
Gua-Mn	23.5	28.2	10.8	2.2	0.30	1.5	11.5	2.41	27.04
Gua-Fe	27.4	30.2	11.5	2.4	0.32	1.9	10.2	2.18	22.32
Gua-Co	29.0	35.7	13.8	2.1	0.30	2.0	8.5	2.45	20.87
Gua-Ni	64.1	40.7	14.6	4.4	0.4	35.6	215.6	0.05	10.47
Gua-Cu	26.1	30.0	11.4	2.3	0.3	10.4	5.0	5.03	25.32
Gua-Zn	30.3	34.2	13.0	2.3	0.3	5.0	8.2	2.46	20.04
EA-Mg	33.7	34.2	12.9	2.6	0.33	21.1	1.9	6.72	12.76
<u>DMA-Co</u>	32.5	31.3	11.7	2.8	0.34	11.4	2.6	6.85	17.54
DMA-Mn	20.9	23.8	9.0	2.3	0.32	6.3	3.2	8.51	26.90
DMA-Zn	31.7	28.2	10.4	3.1	0.35	15.3	3.6	5.36	19.55
HONH ₃ -Mn	15.3	27.5	11.5	1.3	0.20	-0.2	3.7	11.33	41.90
HONH ₃ -Co	26.8	36.9	14.5	1.8	0.27	7.0	3.2	7.18	23.08
HONH ₃ -Ni	8.5	21.7	10.1	0.8	0.08	-8.4	-2.2	-188.08	405.43
HONH ₃ -Fe	22.0	34.0	13.6	1.6	0.24	3.9	3.7	7.63	28.34
HONH ₃ -Zn	28.0	33.8	13.0	2.2	0.30	9.1	2.2	7.51	16.72
HONH ₃ -Mg	24.5	41.2	16.9	1.5	0.22	-0.7	2.7	8.72	23.35
MA-Co(P2 ₁ /c)	19.9	21.1	8.0	2.5	0.32	12.4	-1.8	-32.24	59.26
MA-Mn(P2 ₁ /c)	23.7	23.4	8.8	2.7	0.34	17.8	-210.5	-0.15	32.22
<u>MA-Ni(Pnma)</u>	27.8	23.1	8.5	3.3	0.35	8.6	6.3	1.96	22.48
MA-Zn(P2 ₁ /c)	29.7	27.5	10.2	2.9	0.35	20.9	11.7	4.22	26.36
HAZ-Co	30.1	31.5	11.9	2.5	0.33	18.6	12.6	1.77	22.30
HAZ-Mn	24.8	23.1	8.6	2.9	0.35	15.6	-20.0	-1.73	34.68
HAZ-Zn	28.6	28.8	10.8	2.6	0.33	16.9	32.3	0.82	26.56
HAZ-Mg(Pna2 ₁)	30.2	31.3	11.8	2.6	0.33	19.6	6.1	3.28	19.88
<u>HAZ-Mg(P2₁2₁2₁)</u>	36.2	34.7	12.9	2.8	0.34	6.6	2.3	5.28	13.56
FA-Mn	22.8	25.4	9.6	2.4	0.32	-6.1	53.6	1.07	58.19
NH ₄ -Co	33.9	32.0	11.9	2.8	0.34	3.9	-9.8	-1.73	16.92
NH ₄ -Fe	29.5	27.8	10.3	2.9	0.34	2.5	-4.7	-4.50	21.31
NH ₄ -Mn	18.5	15.1	5.5	3.4	0.36	0.7	-0.9	-439.63	381.82
NH ₄ -Zn	34.7	31.5	11.7	3.0	0.35	6.2	-8.2	-2.04	16.69

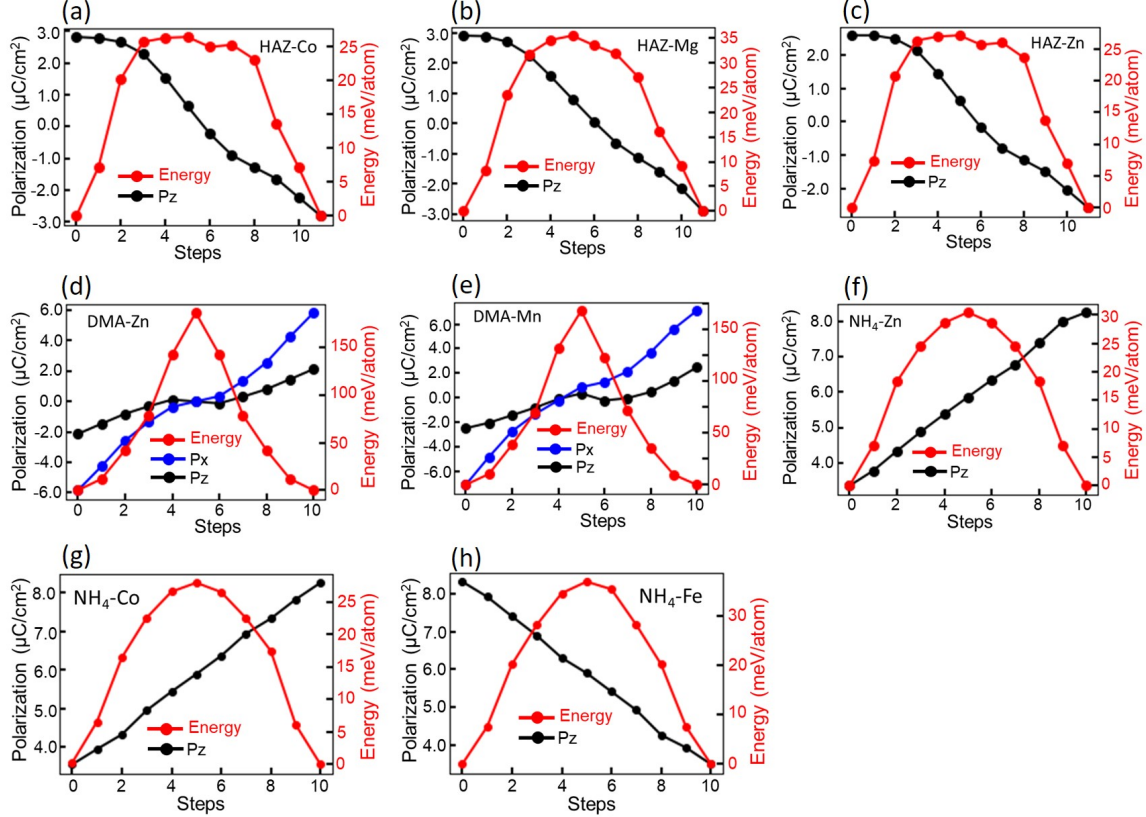


FIG. S1. Variation of polarization and energy along the path for (b) HAZ-Co (c) HAZ-Mg; (d) HAZ-Zn (e) DMA-Zn (f) DMA-Mn (g) NH₄-Zn (h) NH₄-Mn (i) NH₄-Fe

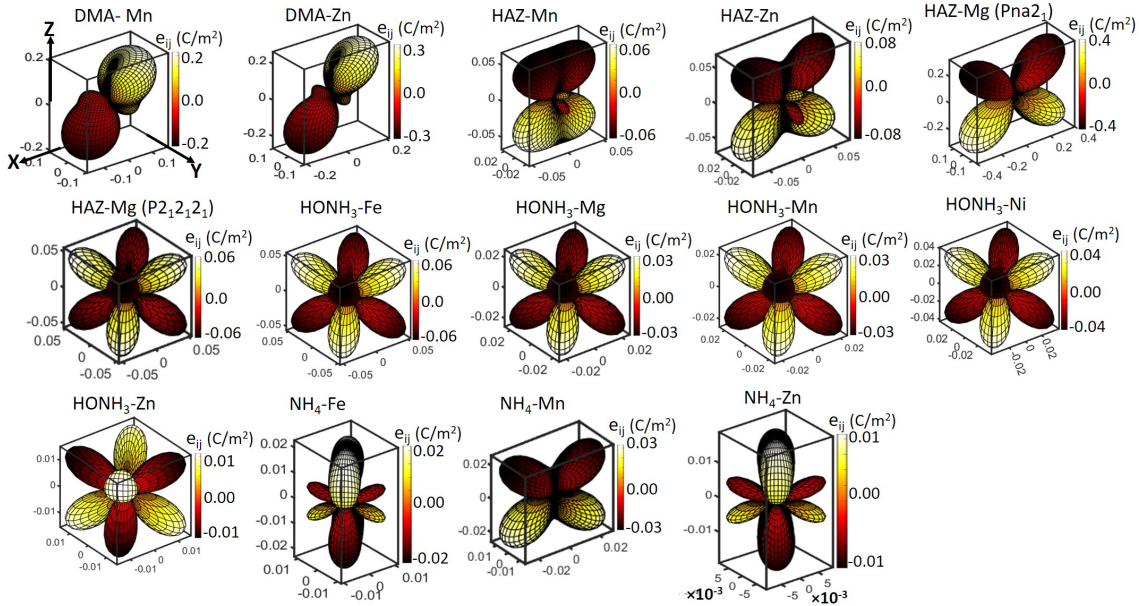


FIG. S2. Piezoelectric stress surface for some of the formates studied in this work, as indicated in the titles.

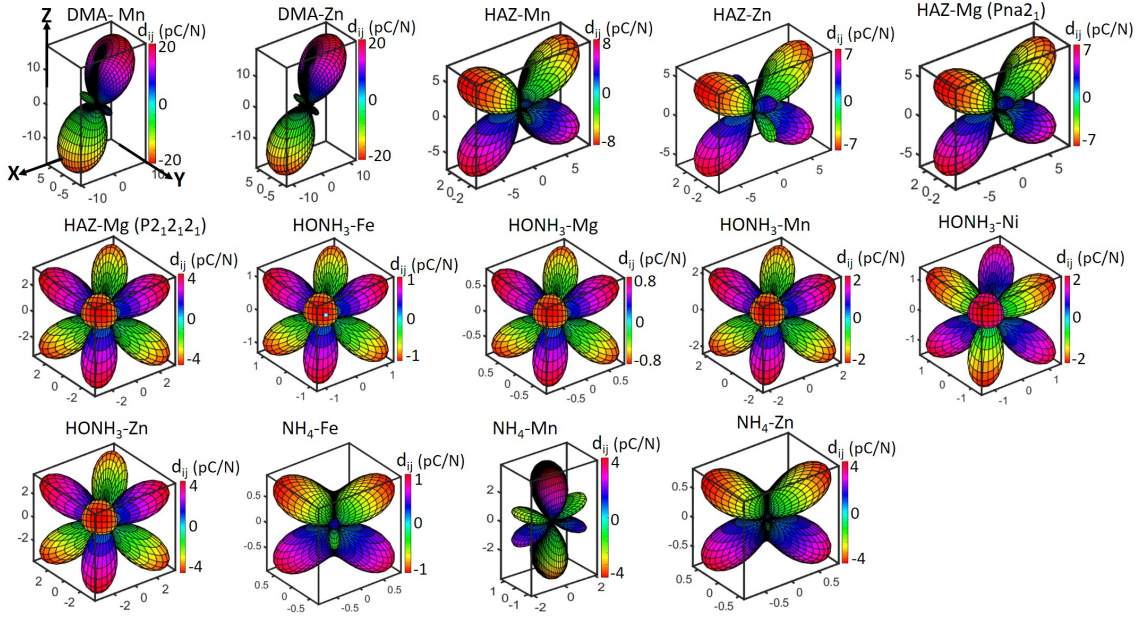


FIG. S3. Piezoelectric strain surface for some of the formates studied in this work, as indicated in the titles.

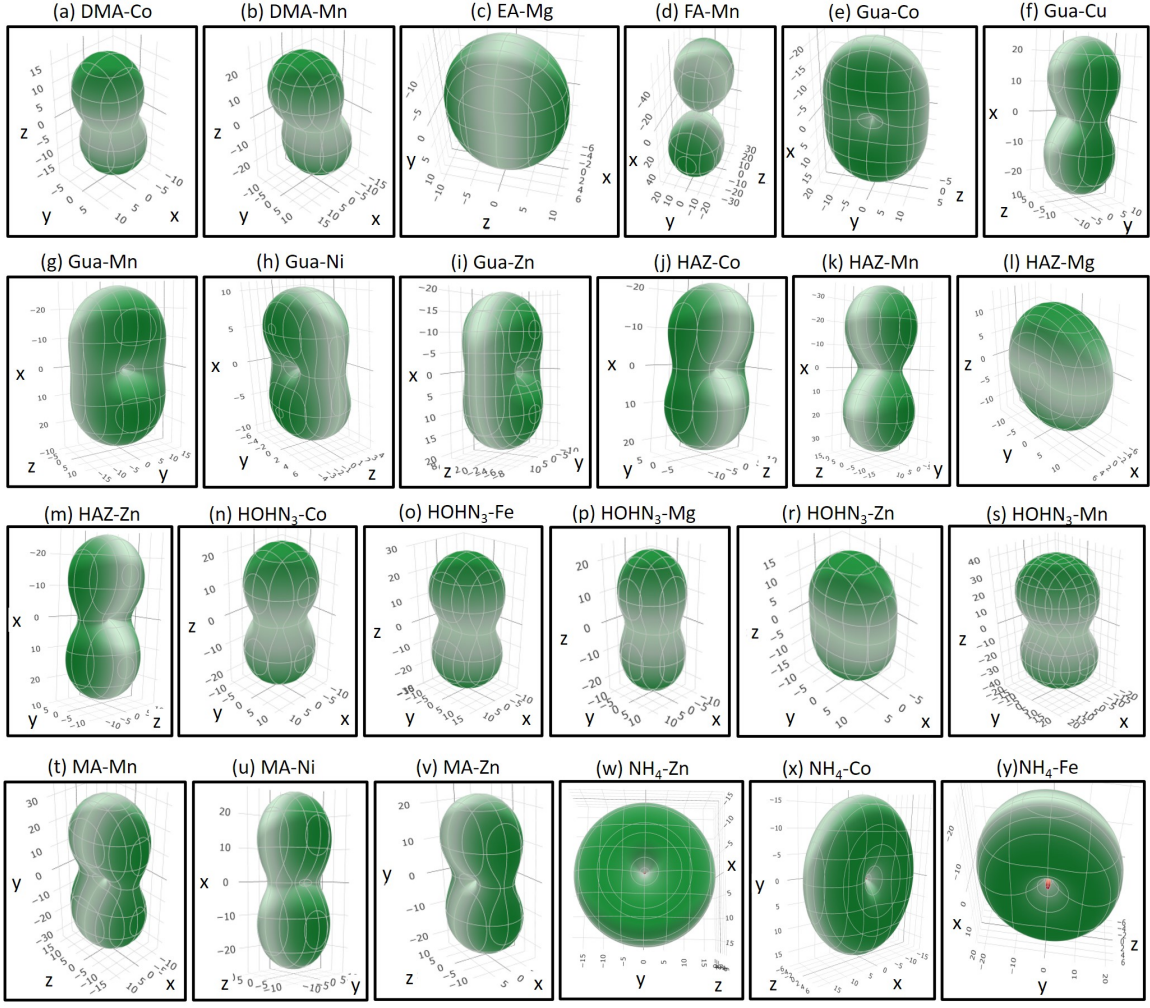


FIG. S4. 3D plots of linear compressibility for some of the formates studied in this work, as given in the titles. Green and red colors correspond to positive and negative values, respectively.